Characterizing RyR and SERCA function in the C57 and D2 *mdx* mouse models of Duchenne Muscular Dystrophy

Riley E.G. Cleverdon, B.Kin

Submitted in partial fulfillment of the requirements for the degree
Master of Science in Applied Health Sciences
(Health Sciences)

Faculty of Applied Health Sciences, Brock University
St. Catharines, Ontario

Abstract

Duchenne Muscular Dystrophy (DMD) is a male-affected muscle wasting disease caused by the complete loss of the sarcolemmal protein dystrophin. No cure exists and patients typically succumb to cardiorespiratory issues in the third or fourth decade of life. Dystrophin loss also leads to dysfunction in other pathways; including impaired sarcoplasmic reticulum (SR) calcium (Ca^{2+}) handling, further perpetuating the disease. This thesis examined potential differences in SR Ca^{2+} handling in two mouse models of DMD. The D2.B10-*Dmd*^{mdx}/J (D2 *mdx*) mouse has emerged as a more pathologically representative model of DMD than the C57BL/10ScSn-*Dmd*^{mdx}/J (C57 *mdx*) mouse model, showing greater muscle weakness, wasting and earlier disease onset. However, SR Ca^{2+} has not yet been characterized in the D2 *mdx* mouse. Thus, the aim of this study was to compare SR Ca^{2+} handling in the D2 *mdx* and C57 *mdx* mice. Using age-matched (9-10 week-old) mice, we found that D2 *mdx* mice had less mass, smaller gastrocnemius muscles, and were less ambulant. The D2 *mdx* mice had significantly higher energy expenditure and respiratory exchange ratio compared with the D2 WT mice. Two separate SR Ca^{2+} uptake assays revealed that D2 *mdx* mice have less Ca^{2+} uptake and leak, and higher starting myoplasmic Ca^{2+}. SERCA activity (ATP hydrolysis) was lower in D2 *mdx* mice while higher in C57 *mdx* mice. These dramatic impairments in SR Ca^{2+} handling were not attributed to differences in SERCA isoform content or changes in its regulator, sarcolipin. However, under reducing conditions, protein nitration and nitrosylation content were significantly higher in D2 *mdx* gastrocnemius muscles. Further, pre-treatment with dithiothreiotol (DTT) did not improve SR Ca^{2+} handling in these muscles, suggestive of irreversible reactive oxygen/nitrogen post-translational modifications. Finally, calpain proteolytic activity was examined to determine the consequence of the impaired SR Ca^{2+} handling in the D2 *mdx* mouse. While D2 WT mice already had higher levels of calpain

activity, the D2 *mdx* mouse had significantly higher calpain activity vs the C57 *mdx* mouse. Altogether, the results from this thesis suggest that impaired SR Ca^{2+} handling may be partially responsible for more severe pathology found in the D2 *mdx* mice.

Acknowledgements

Dr. Val A Fajardo

To Val, thank you for being an amazing role model, mentor, and the greatest support. I am so thankful that you took me on for my masters, without you I would have never found my passion for muscle physiology research. My switch into the Fajardo lab intersected with a 5-month lab shut down from covid, making me worried if I would learn our lab techniques in enough time to graduate. With your guidance I was up to speed in no time, I couldn't imagine making the progress I made without your help. Your passion for science and your belief in your team is infectious and has created such an amazing environment to learn in. In the infamous words of Val: "I'm SERCA pumped!" … to have had you as my mentor and I can't wait to see what you do next. I know it will be big! Thank you.

Family and Friends

Thank you to my mom and dad for shaping me into the person I am today. You both have so selflessly put us kids first in your lives and I owe a large part of my success to you. Thank you for believing in me and to never give up on the things that I love. Thank you for your endless support. I love you both so much.

To Danny, thank you for always being my greatest support, best friend, and partner for the past three years. I'm so glad we have each other to do this with - both grad school and life. It's truly something special. There's no one else I rather crush a long day in the lab with and then go get ice cream with after. Thank you for keeping me sane and challenging me to be the best I can be. I'm so excited to continue sharing this journey with you at McMaster. I love you and here's to us!

To my sisters, Kelsey and Jamey, I love you both so much. I'm fortunate to have you both to come home to and hangout with after long weeks at school. I am so proud of you both and watching you continue to grow and become amazing women you are.

To my Nan and Pop, thank you for your support and love, I will always be grateful for making sure I'm well taken care of. To my grandma and grandpa, I hope that I make you proud, I always know you are looking out for me from above.

Thank you to my kin family, thank for endless laughs, tears (from laughing), love and support. From study dates, to hiking, to ice cream and cottage trips, there's no people I rather spend my time with. I'm so proud of all of us as we pursue of graduate degrees and beyond, look at us go!!!

Thank you to my friends and mentors in the lab, you have all been paramount to my sanity in the lab. I will fondly remember all our Sky Bar excursions. A special shout-out to Kirsten for being my long-time mentor in the lab.

Committee Members and Mentors

Thank you to my committee members, Dr. Rebecca MacPherson and Dr. Brian Roy. Not only am I thankful for your flexibility to my changes in project and your mentorship, but also getting to know you both throughout my years at Brock. Thank you to Becca for all your advice/letting me babysit Henry and to Brian for introducing me to the sport of dragon boating. Thank you to Dr. Ward for introducing me to research and starting my research career. Thank you to all the other incredible researchers and mentors I have met along the way, you have all been instrumental in my development as a researcher.

Lab Members and Cairns Researchers

Thank you to all the students and researchers in Cairns that have taught me and mentored me throughout the years. Lastly, a huge thank you to my lab mates. A later start with my project and covid-related delays made my situation tricky, but all your help and friendship made my experience unforgettable. There's no team I rather be a part of, thank you for becoming my lab family! I'll remember all the coffee runs, blotting support and shanking a few golf balls together at Brock golf. Iconic.

Abbreviations

AMPK	AMP-activated protein kinase
BCA	Bicinchoninic acid
BL10-*mdx*	C57BL/10ScSn-*Dmd*^{mdx}/J
Ca^{2+}	Calcium
CaM	Calmodulin
Calstabin	Calcium channel stabilizing protein
C57 *mdx*	C57BL/10ScSn-*Dmd*^{mdx}/J
DHPR	Dihydropyridine receptor
DTT	Dithiothreitol
DMD	Duchenne Muscular Dystrophy
DMD	Dystrophin gene
DGC	Dystrophin-glycoprotein complex
D2 *mdx*	D2.B10-*Dmd*^{mdx}/J
EBD	Evans blue dye
ECC	Excitation-contraction coupling
ECM	Extracellular matrix
EDL	Extensor digitorum longus
HSP72	Heat shock protein 72
LTBP4	Latent TGFβ binding protein 4
Mg^{2+}	Magnesium
mPTP	Mitochondrial permeability transition pore
NRT1	Nuclear respiratory factor-1
PLN	Phospholamban
RONS	Reactive oxygen/nitrogen species
ROS	Reactive oxygen species
RER	Respiratory exchange ratio
RyR	Ryanodine receptor
SERCA	Sarco(endo)plasmic reticulum Ca^2+-ATPase
Sgcb-/-	β-sarcoglycan deficient mice
SLN	Sarcolipin
SR	Sarcoplasmic reticulum
TBST	Tris-buffered saline tween solution
TGFβ	Transforming growth factor beta
WT	Wild type

Table of Contents

Chapter 1: Literature Review

1.1 Duchenne Muscular Dystrophy

Duchenne Muscular Dystrophy (DMD) is an X-linked recessive severe muscle-wasting disorder that affects approximately 1 in 3500 boys worldwide [1,2]. Onset of clinical symptoms in these boys occurs around 3 to 4 years of age and leads to wheelchair dependence by 7 to 13 years of age [3,4]. When DMD boys reach approximately 20 years of age, they enter the terminal stages of the disease and require ventilation [5]. There is currently no cure for DMD and patients often succumb to cardiac and/or respiratory failure due to their disease around 30 to 40 years of age [5,6].

DMD is caused by mutations in the *DMD* gene, a 79-exon gene which codes for the protein dystrophin. Over seven thousand mutations exist which result in non-functional dystrophin protein [7,8]. Numerous large and small mutations of the *DMD* gene may occur, and 80% of mutations can be attributed to large mutations (1 exon or larger) while 20% arise from small mutations (< 1 exon) (Table 1.1). Of the large mutations, deletions account for several thousand mutations, while duplications compose several hundred. Small mutations are induced most commonly by point mutations, small deletions, small insertions and affected by splice site. Less common small mutations include missense and mid-intronic mutations.

Table 1.1: Known Mutations of the DMD gene causing Duchenne Muscular Dystrophy.

Large Mutations (1 exon or larger)		
	Number of Known Mutations	**% of Total LARGE Mutations**
Deletions	4894	86%
Duplications	784	14%
Total Large Mutations	**5682**	**80% of Total Mutations**
Small Mutations (< 1 exon)		
	Number of Known Mutations	**% of Total SMALL Mutations**
Small Deletions	358	25%
Small Insertions	132	9%
Affected by Splice Sites	199	14%
Point Mutations	756	52%
Missense Mutations	30	2%
Mid-Intronic Mutations	22	0.3%
Total Small Mutations	**1445**	**20% of Total Mutations**
Total Known Mutations	**7149**	

Under normal physiological conditions, dystrophin is a cytoplasmic protein which connects the cytoskeleton and extracellular matrix of a muscle fibre, linking it directly to the sarcolemma [9]. Dystrophin combines with other proteins to form the dystrophin-glycoprotein complex (DGC), which is involved in the structural integrity of the muscle cell membrane [9]. However, when functional dystrophin is absent as in the case of DMD, it will lead to the loss of the DGC which can cause membrane tearing and myofibre damage/degeneration. Healthy skeletal muscles can regenerate damaged myofibres through the activation of normally quiescent cells called satellite cells. Upon activation, satellite cells proliferate and either self-renew or differentiate to become muscle precursor cells called myoblasts that can mature and fuse with damaged muscles [10]. In early stages of the disease, muscle regeneration is evident in DMD patient biopsies through the observation of small, immature centrally nucleated fibres [11,12]. This enhancement of muscle regeneration aims to offset the degenerative nature of the disease. However, as

the disease progresses, the ability to regenerate declines [13] and fibrous extracellular matrix (ECM) and adipose tissue replace muscle fibres, shifting the balance in favour of necrosis.

Like other forms of muscular dystrophies, DMD is characterized by an increase in central nuclei, fibre size variability, serum creatine kinase (CK) levels, progressive fibrosis, fat infiltration and muscle weakness [14]. Though the loss of functional dystrophin is the primary cause of disease in DMD, several secondary consequences including chronic inflammation, oxidative stress, and Ca^{2+} overload (discussed below), ultimately lead to the pathologic degeneration/failed regeneration, necrosis and fibrotic/fatty tissue replacement of muscular tissue [15].

1.2 The role of Ca^{2+} in DMD

Ca^{2+} is a potent signaling and regulatory molecule in all cells. In resting skeletal muscle, intracellular Ca^{2+} levels ($[Ca^{2+}]_i$) levels are relatively low ~10^{-7} M or 100 nM [16]. During excitation-contraction coupling (ECC) as exemplified in *Figure 1.1*, depolarization of the surface membrane (A) travels down into invaginations of the membrane called transverse-tubules (t-tubules) [17]. There, L-type voltage gated Ca^{2+} release channels, dihydropyridine receptors (DHPR) sense the change in membrane charge (B), and through a mechanical interaction, relays this information to the ryanodine receptor (RyR) found within the sarcoplasmic reticulum (SR) membrane (C) [18]. This leads to the rapid release of Ca^{2+} out from the SR (D) and through RyR [19], and can reach intracellular Ca^{2+} levels of up to 20 μM [20]. As increased Ca^{2+} enters the cytosol, Ca^{2+} binds to the troponin complex ultimately moving tropomyosin from the globular (G)-actin sites of the thin filament (E) [16]. The exposure of the G-actin sites allow the thin and thick filament to

engage in cross-bridge formation initiating muscle contraction [16]. After contraction, the sarco(endo)plasmic reticulum Ca^{2+}+ ATPases (SERCA) actively transports Ca^{2+} from the cytoplasm back into the SR (F) where it binds to calsequestrin (G) thereby returning $[Ca^{2+}]_i$ to resting levels [21]. This is important because aside from ECC, Ca^{2+} regulates several other pathways including energy expenditure, second messenger signaling, activation of transcription factors, and apoptosis [22]. If $[Ca^{2+}]_I$ become chronically elevated, it can impart negative effects leading to muscle damage and weakness.

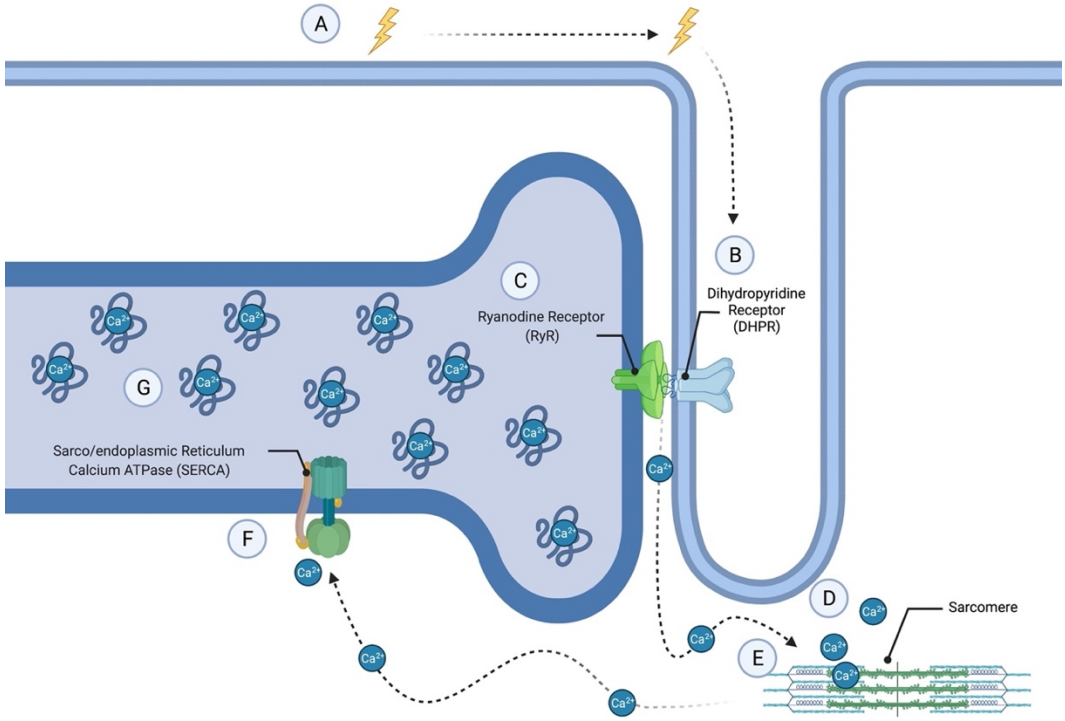

Figure 1.1: Normal SR Ca2+ handling in skeletal muscle. Created with bioRender.

It is widely accepted that membrane instability causes a subsequent chronic influx of Ca^{2+} into the muscles of patients living with DMD. The resulting Ca^{2+} overload exacerbates oxidative stress, inflammation, and cellular necrosis thereby perpetuating dystrophic pathology [23,24]. Ca^{2+}-induced muscle necrosis occurs through at least two distinct mechanisms: 1) the activation of the Ca^{2+}-sensitive protease, calpain and; 2)

mitochondrial swelling and rupture. As a result of the elevated $[Ca^{2+}]_i$, proteolytic calpain activation is heightened in muscular dystrophy leading to excessive protein degradation and thus muscle loss. Transgenic overexpression of calpastatin, a specific inhibitor of calpains has been shown to decrease muscle necrosis, muscle lesions all while reducing the number of actively regenerating muscle fibres in the *mdx* mouse – the traditional mouse model of DMD [25]. The mitochondria also contributes to intracellular Ca^{2+} regulation, however, in conditions of Ca^{2+} overload, the mitochondria will excessively take in Ca^{2+} leading to the mitochondrial permeability transition pore opening and intrinsic apoptosis [26]. Thus, Ca^{2+} dysregulation is a well-known pathological contributor in DMD. Though the initial cause of Ca^{2+} overload in DMD is membrane instability, impairments in SR Ca^{2+} handling (ie. RyR and SERCA dysfunction) can also contribute to muscle weakness and pathology.

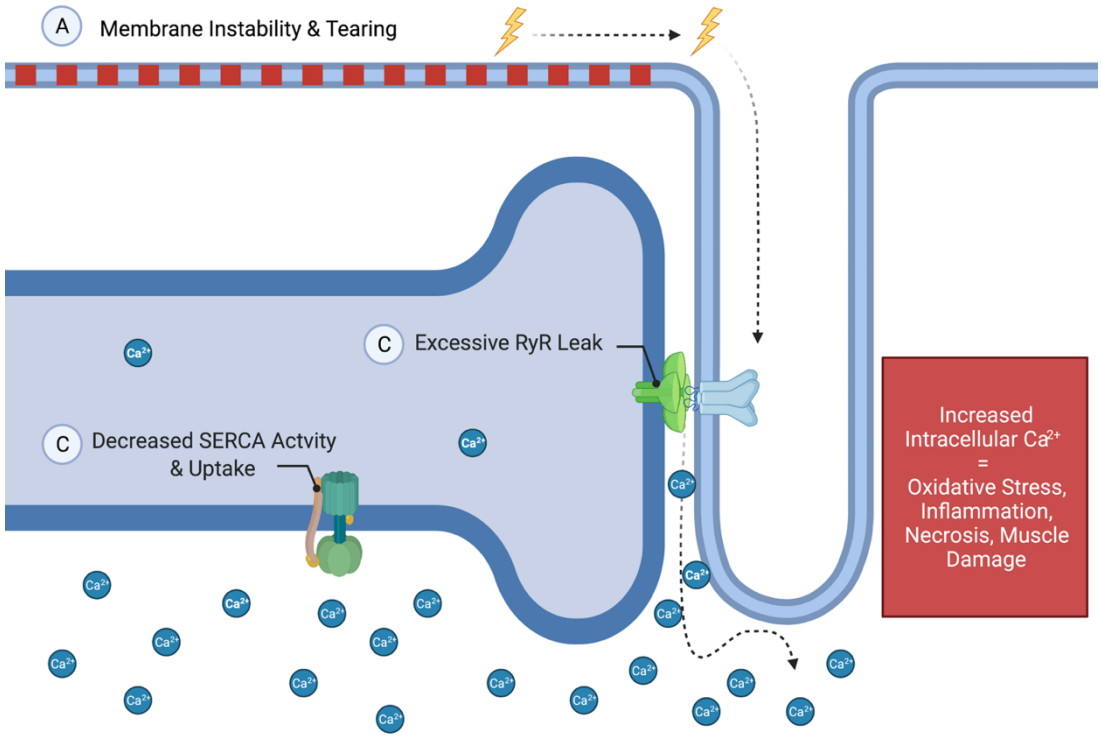

Figure 1.2: The SR calcium hypothesis of DMD. Created with bioRender.

1.3 Healthy RyR function

RyRs are the largest known ion channels, containing approximately 5000 amino acid residues (565 kDa) per tetramer, resulting in a total weight of over 2.2 MDa [27,28]. RyRs consist of a transmembrane domain which forms an ion-conductive pore and a large N-terminal cytoplasmic domain [28]. There are three known isoforms of mammalian RyR; RyR1, RyR2 and RyR3. RyR2 is the cardiac isoform [29–31], and RyR3 is ubiquitously expressed [32–35]. Though RyR3 has been found in skeletal muscle, it does not appear to play a role in ECC and its exact function is not yet well understood [36]. Conversely, RyR1 is the dominant and most important isoform found in skeletal muscle, and will therefore be the focus of this review/proposal [28,37,38].

RyR and DHPR orientation

In skeletal muscle, ECC is dependent on the physical interaction between DHPR and RyR1. DHPR, the main effector of RyR1, interacts with the cytoplasmic domain (or foot) of RyR1 in a tetradic arrangement via DHPR loops (Figure 1.1) [39]. It is known that these loops are critical for relaying the electrical signal of an action potential to a mechanical one causing Ca^{2+} release through the RyR1 channels. In this respect, the α_{1S} II-III loop of DHPR have a critical role in conformational coupling with RyR1, however its specific mechanism remains to be elucidated [39]. In muscle, the DHPR tetrads do not completely occupy all RyR1 cytoplasmic feet, giving rise to a ‘checkerboard’ pattern of orientation (Figure 1.1). Thus, the number of DHPR linked with RyR1 is an important factor in Ca^{2+} gating and release.

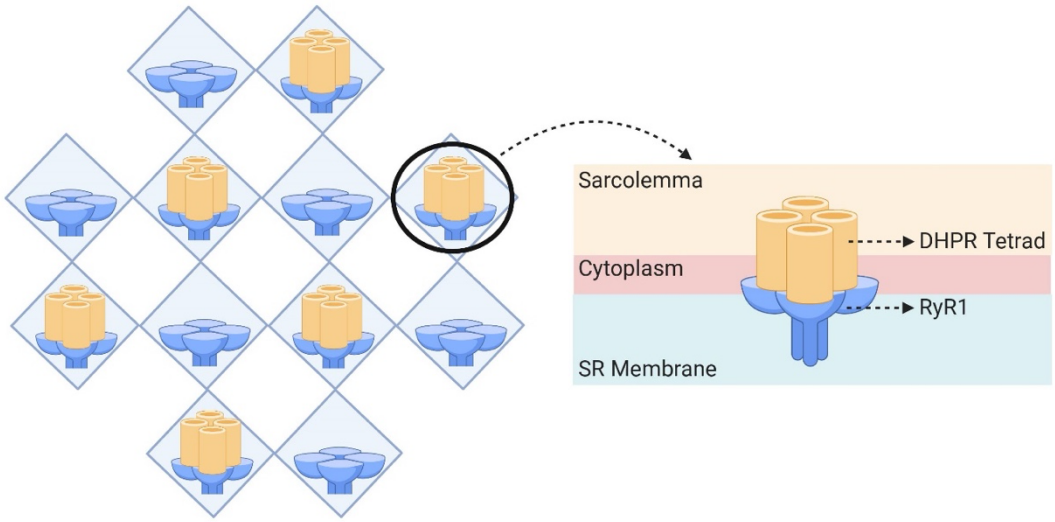

Figure 1.3: RyR and DHPR orientation. RyR is organized in a tetramer with each 'foot' protruding out towards the cytosol. A DHPR tetrad faces the RyR foot and is connected through cytoplasmic loops (not shown here). Created with bioRender.

Muscles that have more RyR1 linked to DHPR will have a greater capacity to release Ca^{2+} and at a much faster rate compared with muscles that have relatively less RyR1 and DHPR. This is best exemplified when comparing the various fibre types that can be found within skeletal muscle. Slow-twitch (type I) fibres exert slow, prolonged, and less forceful contractions and they exhibit high oxidative (ie. mitochondrial content/respiration) capacity making them fatigue resistant. Conversely, fast-twitch (type II) fibres exert fast and more forceful contractions; however, their contractile and metabolic properties can be further sub-divided. Type IIA fibres have both high oxidative and glycolytic potential but are generally slower than the fast-glycolytic type IIX and IIB fibres. Notably, type IIB fibres are not present in human skeletal muscle but can be found in rodent skeletal muscle [40]. Differences in RyR1 content and orientation with DHPR can contribute to the differences in contractile properties between slow and fast fibre types by altering the rate and amount of Ca^{2+} release. Research has shown that slow twitch

muscles contain lower amounts of total RyR1 and RyR1 linked to DHPR [41,42] (Figure 1.2).

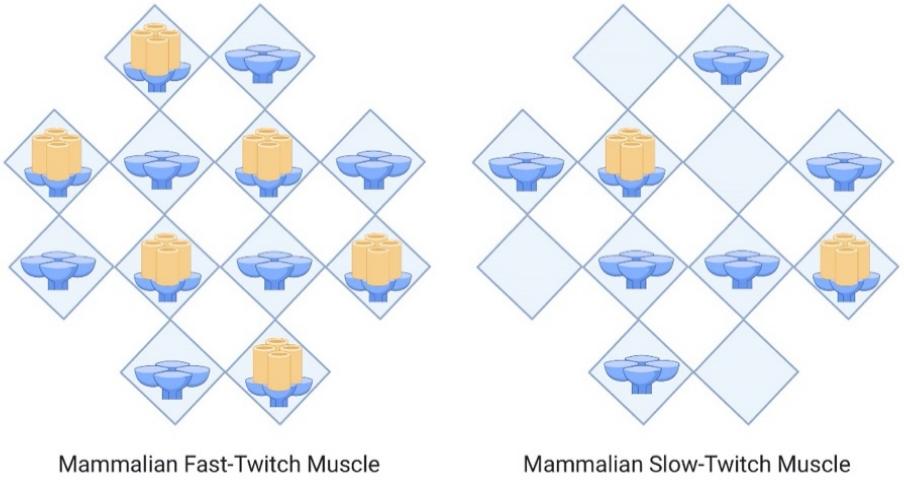

Figure 1.4: Fiber type differences in RyR and DHPR expression. Mammalian fast-twitch fibres have higher RyR1 content and greater ratio of linked RyR1 to DHPR in comparison to slow-twitch fibres, leading to differences in contractile function. Created with bioRender.

Thus, muscles that have a large proportion of slow fibres such as the soleus will release less Ca^{2+} and at a much slower rate upon excitation compared with muscles that are dominated by fast twitch fibres such as the extensor digitorum longus (EDL) (Figure 1.3). These differences in the Ca^{2+} amplitude and Ca^{2+} transient are directly in line with the known differences in the amount and rate of force produced between these muscles (Figure 1.3).

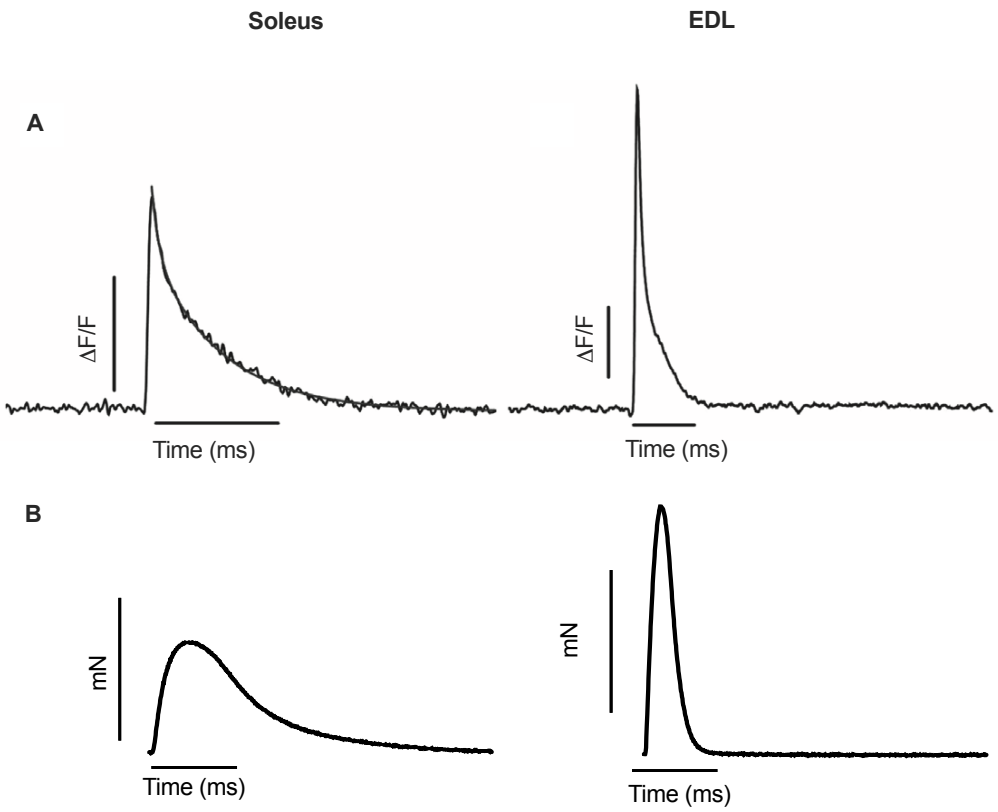

Figure 1.5: Twitch Ca^{2+} and force tracings from rodent soleus and extensor digitorum longus (EDL) muscles. A) Single Ca^{2+} transients from fibres obtained from soleus and EDL muscles loaded with the Ca^{2+} fluorescent indicator Magfluo-4AM [43]. As depicted, EDL muscles have a larger Ca^{2+} amplitude, and shorter rise time. Previous studies have shown that rat slow fibres have a peak $[Ca^{2+}]_i$ of 9 μM compared with the 19 μM in fast fibres; and 1.3 μM in slow fibres vs. 2.4 μM in fast fibres using fura-2 as a Ca^{2+} fluorescent indicator [20]. B) Force tracings from intact soleus and EDL muscles from our lab (unpublished data) showing the greater force and faster twitch kinetics in the EDL.

Regulation of RyR

In addition to its primary effector DHPR, many factors can regulate RyR – including Ca^{2+}, magnesium (Mg^{2+}), caffeine, calmodulin (CaM), calcium channel stabilizing binding protein (calstabin), and various post-translational modifications. Micromolar cytosolic levels activate the channel while millimolar levels inhibit the channel. This biphasic behaviour can be explained by the presence of two binding sites for Ca^{2+} on RyR: one with moderate-affinity, which activates RyR opening, and another with low-affinity which inhibits opening when $[Ca^{2+}]$ become too high [44]. Further, Mg^{2+} can also modulate the

effect of Ca^{2+} on RyR acting as a competitive antagonist of Ca^{2+} thereby inhibiting RyR opening at physiological concentrations [45]. At 1 mM, Mg^{2+} decreases the binding affinity of Ca^{2+} from 1 μM to 50 μM [46]. Conversely, caffeine acts as an allosteric agonist of Ca^{2+}, and the addition of caffeine to SR vesicles results in an increase of open probability of RyR [47] by enhancing Ca^{2+} binding sensitivity [48].

Calstabin is an immunophilin that has a high affinity to bind to the tetramers of the RyR1 complex at a ratio of one calstabin to each monomer (Figure 1.4). Calstabin stabilizes the closed state of the channel, coordinating gating behaviour of RyR1 opening during muscle contraction and preventing intracellular Ca^{2+} leak [49–51]. Ca^{2+} leaks are spontaneous Ca^{2+} release events originating from the uncontrolled opening RyR.

CaM is a ubiquitous Ca^{2+}-binding protein that can modulate proteins through direct binding and/or activation of CaM-dependent protein kinases and phosphatases [52]. CaM in the Ca^{2+} free state (apo-CaM) and Ca^{2+} bound state (Ca^{2+}/CaM) binds directly to RyR to influence channel function [53]. At nanomolar Ca^{2+} concentrations, apo-CaM acts as a feed forward mechanism, and activates RyR1 opening. However, when Ca^{2+} reaches micromolar concentrations, Ca^{2+}/CaM acts as a negative feedback loop and inhibits RyR1 opening [54]. In addition, CaM activation of Ca^{2+}/CaM-dependent kinase II (CaMKII) can increase phosphorylation of RyR1 leading to increased Ca^{2+} release. Phosphorylation of RyR1 can also occur with protein kinase A (PKA) at which can be activated with β-adrenergic signaling and exercise. Specifically, it has been shown that PKA and CAMKII mediated phosphorylation at Ser2843 of RyR1 causes the release of calstabin from RyR thereby increasing channel activity [55,56]. Importantly, hyperphosphorylation of RyR1 leads to excessive Ca^{2+} leak impairing SR Ca^{2+} release leading to fatigue and exercise intolerance [57].

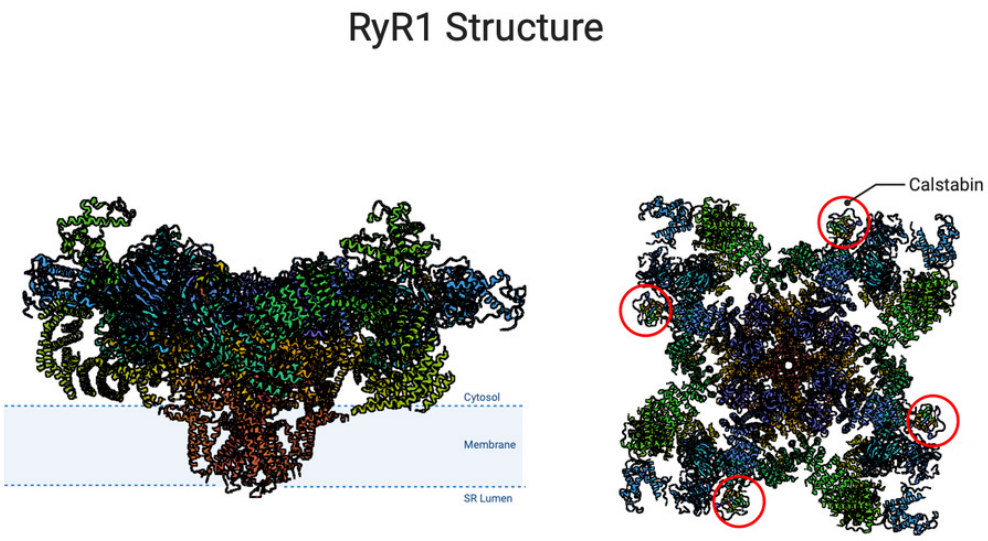

Figure 1.6: 3-D protein shape of RyR1. Four calstabin are bound to RyR1 and are highlighted by red circles surrounding the protein. Created with bioRender.

Finally, the redox state of RyR regulates its structure and function to either activate or inactivate the channel, affecting subsequent Ca^{2+} signaling [58,59]. RyRs are sensitive to reactive oxygen/nitrogen species (RONS) such as endogenous free radicals superoxide ($O2^{-}$) and nitric oxide (NO). This is due to the presence of multiple sulfhydryl groups on cysteine residues on the RyR complex making the structure susceptible to post-translational modifications, including cysteine (S)-nitrosylation [60,61]. Peroxynitrite ($ONOO^{-}$), formed through a reaction of O_2- and NO [62] can result in S-nitrosylation of residues RyR1-Cys-3635 and RyR1-Cys2327, which has been shown to increase RyR1 channel activity and Ca^{2+} leak through a decrease in calstabin binding (to RyR1) [60,63]. The interaction between oxidative/nitrosative agents which act on RyR are important regulators in the physiological and pathophysiological function of the channel.

1.4 RyR and DMD pathology

While the initial insult in DMD leading to Ca^{2+} overload is membrane instability, several studies have shown that impaired RyR function also contributes to Ca^{2+} dysregulation, muscle weakness, and dystrophic pathology. Specifically, excessive RyR1 Ca^{2+} leak has been observed [64,65]. This leak has been found to be caused by both calstabin depletion and elevated S-nitrosylation of RyR1, whereas the role of PKA-mediated phosphorylation at Ser2483 in dystrophic pathology remains unclear [65].

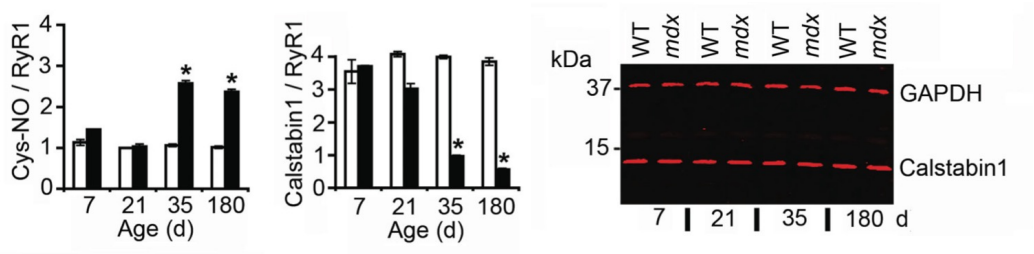

Figure 1.7: RyR is S-nitrosylated and subsequently depleted of calstabin in mdx mice [65].

Importantly, treating C57BL/10ScSn-*Dmd*^{mdx}/J (C57 *mdx*) mice with Rycal S107, a drug that enhances RyR-calstabin binding, reduced Ca^{2+} leak, calpain activation, and ultimately alleviated the histopathology and muscle weakness found in these mice [65]. Aside from DMD, leaky RyR channels are a common event across other muscular dystrophies. In β-sarcoglycan deficient mice (Sgcb-/-), a model of Limb-Girdle muscular dystrophy, RyR channels were found to be nitrosylated and oxidized. Along with calstabin depletion, this altogether corresponded with increased RyR open probability [64]. In addition, S107 therapy also had positive outcomes on the dystrophic phenotype in these mice, resulting in improved Ca^{2+} transients, specific muscle force, and exercise capacity [64]. Together, these studies demonstrate the role of RyR leak in dystrophic pathology and that mitigating RyR Ca^{2+} leak can also mitigate muscular dystrophy.

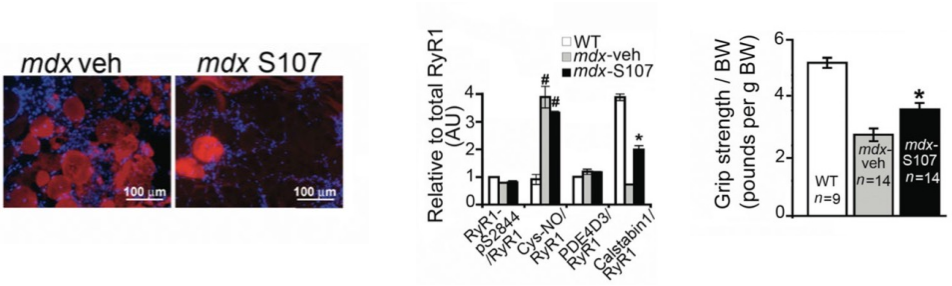

Figure 1.8: Rescuing of RyR leak pharmaceutically with S107 diminishes dystrophic pathology [65].

1.5 Healthy SERCA pump function

SERCA is a 100-110 kDa integral SR membrane protein responsible for maintaining and restoring resting levels of $[Ca^{2+}]_i$ by pumping Ca^{2+} against a near 10,000-fold gradient into the SR using energy derived from adenosine triphosphate (ATP) hydrolysis [66,67]. The SERCA protein structure consists of three cytoplasmic domains (actuator, phosphorylation, and nucleotide binding; collectively referred to as the headpiece), 10 transmembrane domains (M1 through M10), and two high affinity Ca^{2+} binding sites (site I and II), which are located between transmembrane helices M4-M6 and M8 [68–70] (Figure 1.5). Based on binding capacity, SERCA can optimally transport two Ca^{2+} ions into the SR for every 1 ATP hydrolyzed ATP [66]; however, the coupling ratio *in vivo* is much lower. More than 10 isoforms of SERCA exist in vertebrates [66], however, in adult skeletal muscle two isoforms reign – SERCA1a and SERCA2a. Isoform expression is suggested to be reliant on muscle fibre type where SERCA1a is primarily expressed in fast type II skeletal muscle fibers, while SERCA2a is primarily expressed in slow type I muscle fibres in cardiac and skeletal muscle [71]. It should be noted that both isoforms are expressed in type I and type II fibers [72]. Further, though SERCA1a is known as the fast SERCA isoform compared with SERCA2a, the primary determinant in the rate of SR Ca^{2+} uptake is the amount or density of the SERCA pump – to which the fast type II

fibres have more than the slow type I fibres [73]. This ultimately allows for a more rapid rate of Ca^{2+} re-uptake and muscle relaxation in fast muscles such as the EDL compared with the soleus (Figure 1.3).

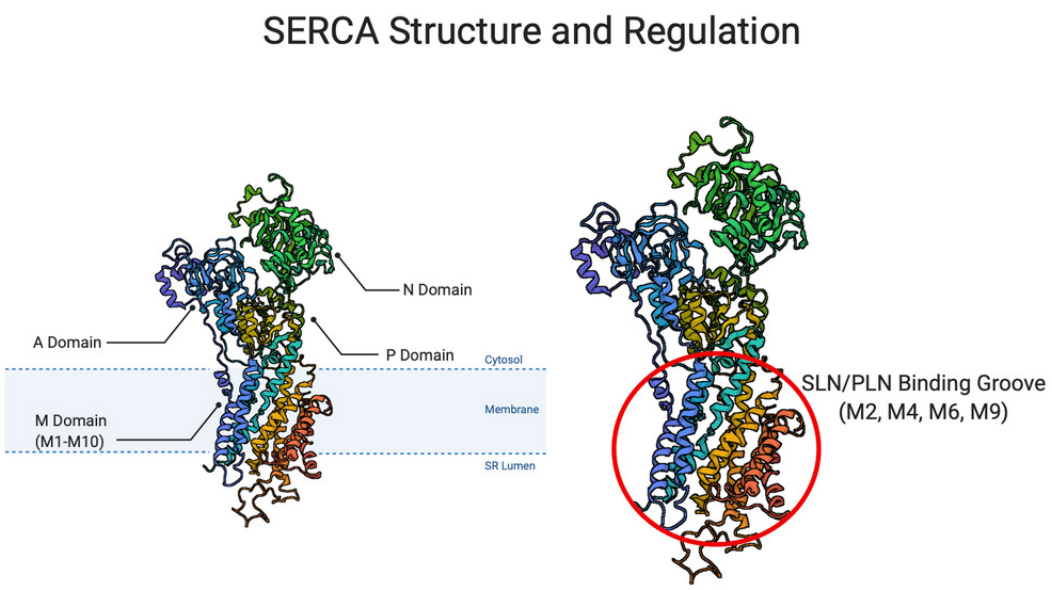

Figure 1.9: SERCA protein structure. The cytoplasmic domain consists of the actuator (A) domain, nucleotide (N) domain, phosphorylation (P) domain. The transmembrane (M) domain consists of M1-M10, and the two Ca^{2+} bindings sites. The binding groove for SERCA regulators, sarcolipin (SLN) and phospholamban (PLN) is also highlighted. Created with bioRender.

Regulation of SERCA

In addition to SERCA pump density, SERCA1a and SERCA2a are predominately regulated by two small molecular-weight proteins, sarcolipin (SLN) and phospholamban (PLN) [66]. Although it has been shown that SLN preferentially regulates SERCA1a and PLN preferentially regulates SERCA2a, SLN and PLN may regulate both isoforms in human skeletal muscle [72]. Both micropeptides function to lower Ca^{2+} binding affinity of SERCA1a/2a to inhibit SERCA-mediated transport [74]; however, SLN has the additional role of uncoupling the SERCA pump and mediating muscle-based thermogenesis.

PLN is most known for its role in regulating SERCA in cardiac muscle. It may become phosphorylated at Ser16 by PKA and Thr17 by CaMKII to relieve its inhibition on SERCA [75,76]. This control mechanism is critical for regulating the inotropic and chronotropic effects of β-adrenergic stimulation to the heart. For example, during the fight-or-flight response PKA mediated phosphorylation of PLN increases SERCA-mediated Ca^{2+}-re-uptake thereby increasing the rate of relaxation and the amount of releasable Ca^{2+} in the SR [77]. Though SLN may also be phosphorylated at Thr5, under regular physiological conditions, SLN is not typically phosphorylated [78] and thus the physiological role of SLN phosphorylation remains unknown.

In addition to SLN and PLN, RONS can also regulate SERCA function. SERCA contain sensitive cysteine, tyrosine and lysine residues, making the pump sensitive to post-translational modifications like oxidation, S-nitrosylation and tyrosine (T)-nitration [79–81]. T-nitration and S-nitrosylation have been the most studied thus far. Interestingly, SERCA2a has been shown to be the isoform most susceptible to T-nitration causing to impairments in its function [80,82]. Though SERCA1a may not as sensitive to T-nitration [79,82], both SERCA2a and SERCA1a can also be modulated by peroxynitrite-dependent S-nitrosylation, which has also been shown to inactivate the pump [79,83].

1.6 SERCA and DMD

Similar to RyR, the SERCA pump has also emerged as a therapeutic target for DMD. Impaired maximal Ca^{2+} uptake (V_{max}) and Ca^{2+} affinity of SERCA was reported in the soleus, diaphragm, and quadriceps muscles obtained from the C57 *mdx* mouse model, and the more severe *mdx*-utrophin double knockout model that lacks both dystrophin and its functional homolog utrophin. As expected, both maximal SERCA uptake and SERCA

affinity for calcium were most impaired in the *mdx*-utrophin knockout model compared with the C57 *mdx* and WT mice [84]. Like RyR, impairments in SERCA function have also been observed in other models of muscular dystrophy, including the limb girdle models, Sgcb-/- and dy^{2j}/dy^{2j} [85,86]. Further, studies have shown that upregulating SERCA content in C57BL/6 *mdx* and Sgcb-/- muscles either through transgenic overexpression or adenoviral gene therapy alleviates the dystrophic pathology reducing fibrosis and serum CK and improving muscle force production levels in the diaphragm [85,87]. The reductions in SERCA pump activity and uptake in dystrophic models can be partly attributed to the oxidative/nitrosative stress that can lead to damaging protein modifications. In fact, protecting the SERCA pumps from oxidative/nitrosative stress via transgenic or pharmacological upregulation of the chaperone protein heat shock protein 72 (HSP72) in C57 *mdx* mice improved SERCA function lowering serum CK levels and increasing muscle-specific force [88]. HSP72 has the ability to bind to and protect the SERCA pumps from inactivation due to oxidative/nitrosative stress [89–91].

Though the role of PLN-mediated SERCA regulation in DMD skeletal muscle pathology has yet to be studied, PLN overexpression in murine skeletal muscle causes severe muscle atrophy and a myopathic phenotype that exhibits some dystrophic features [92]. These include heightened Ca^{2+}-activated proteolysis, protein S-nitrosylation, central nucleation, progressive fibrosis, and elevated serum CK. On the other hand, the role of SLN in dystrophic pathology has been recently studied with conflicting results. SLN is upregulated several-fold in muscles obtained from *mdx* mice and is upregulated further in the more severe *mdx*-utrophin double knockout model [84]. Thus, SLN expression increases with disease severity, and with its role as a SERCA inhibitor, is thought to contribute to dystrophic pathology. In agreement with this, SLN deletion in the *mdx*/utrophin double knockout mouse alleviated both skeletal and cardiac muscle

pathology prolonging lifespan in these mice [93]. In the C57BL/6 *mdx* mouse model, genetic deletion of SLN resulted in partial improvements in serum CK levels, grip strength, and treadmill performance [94]. However, in contrast with these previous findings, Fajardo et al., (2018) found that genetic deletion of SLN in the C57BL/6:C57BL10 *mdx* mouse actually worsened the dystrophic pathology with increased serum CK, muscle degeneration, and lowered cage activity [95].

Though the explanation for these discrepant findings remains unknown, it could relate to the level of SERCA improvement observed with SLN deletion. Voit et al., (2017) found that SLN deletion in the *mdx*/utrophin double knockout mouse restored maximal SERCA Ca^{2+} uptake and SERCA's affinity for Ca^{2+} to that of WT levels [93]. Conversely, Fajardo et al., (2018) only found improvements in SERCA's affinity for Ca^{2+} and not maximal SERCA activity when SLN was genetically deleted from C57BL/6:C57BL/10 *mdx* mice [95].

Collectively, these studies show that SERCA function is impaired in DMD and other forms of muscular dystrophy. Restoring SERCA pump activity and Ca^{2+} uptake to healthy WT levels via transgenic overexpression, cytotoxic protection, or in some cases SLN deletion can alleviate dystrophic pathology. Therefore, the SERCA pump plays a critical role in the Ca^{2+} dysregulation that occurs in DMD.

1.8 The D2 *mdx* mouse

The *mdx* mouse is the classical mouse model used to investigate the cellular mechanisms underlying DMD (including but not limited to the roles of SERCA and RyR). It was originally discovered by Bulfield and colleagues (1984) in the inbred line of C57BL/10 mice by which a mutation of exon 23 arose spontaneously, causing an early

termination code and truncation of dystrophin protein [96–98]. Similar to DMD patients, *mdx* mice lack functional dystrophin protein, resulting in the dystrophic phenotype. The majority of *mdx* studies have used the traditional C57 *mdx* mouse. The major limitation to this model is that the pathology displayed does not match the severe, progressive nature of disease seen in human DMD. Pathophysiology like fibrosis, calcification, and necrosis do not appear to progressively worsen in the C57 *mdx* mouse, and severe symptoms including severe muscle weakness, accumulation of fat and fibrosis, muscle weight loss, and shortened lifespan are not present until 2 years of age [99]. In fact, the only muscle largely affected in the C57 *mdx* mouse is the diaphragm, which displays progressive degeneration, and loss of force production [100]. To try and circumvent this limitation, researchers have used the *mdx*/utrophin double knockout model that more closely mimics the phenotype of DMD with respect to disease severity. However, this has its limitations in that it does not genotypically represent DMD cases where the utrophin gene is intact and serves as a compensatory mechanism.

Recently, the C57 *mdx* mouse model was backcrossed onto a DBA/2J strain (D2 *mdx*) and was found to more closely mimic DMD pathology. Specifically, EDL maximum and specific force has been shown to be significantly more reduced in D2 *mdx* mice compared to C57 *mdx* mice [101], and as soon as 7 weeks of age [102]. Diaphragm muscle in C57 *mdx* and D2 *mdx* mice have been demonstrated to undergo similar deficits in specific muscle force [101]. This is accompanied by significantly lower amounts of centrally nucleated fibres [102,103], and significantly less total myofibres by 8 months of age [104]. Unlike the C57 *mdx* mice, muscles from the D2 *mdx* mice do not display pseudohypertrophy and are smaller than their WT counterparts [101]. Evans blue uptake (EBD) is used to measure membrane stability with greater uptake in muscle fibres indicative of heightened muscle damage. Not surprisingly, EBD uptake is much more

extensive in the D2 *mdx* mouse compared with the C57 *mdx* mouse [102]. The percentage of unhealthy tissue, including fibrosis, necrosis and inflammation in D2 *mdx* compared to C57 *mdx* mice was significantly greater in quadriceps, gastrocnemius, triceps, and diaphragm by 10 weeks of age [105] (Figure 1.6). Though cardiac function is not directly related to this proposal, the hearts of D2 *mdx* mice display fibrosis at the early age of 10 weeks of age, and cardiac dysfunction is earlier detected in D2 *mdx* mice compared to C57 *mdx* mice is progressive at 34 weeks of age [102,105].

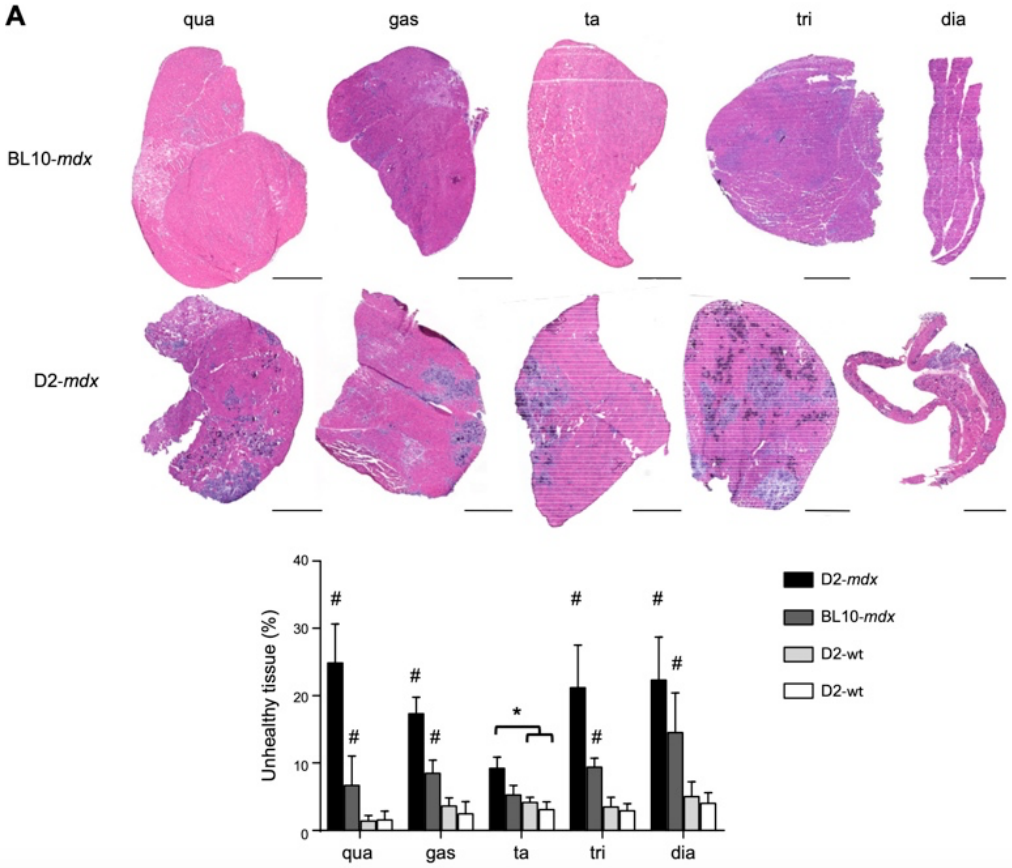

Figure 1.10: Comparison of H&E stained skeletal muscles and quantified unhealthy tissue from 10 week old C57 *mdx* and D2 *mdx* mice (obtained from reference # [105]). By this age, D2 *mdx* quadriceps, gastrocnemius, tibialis anterior, triceps and diaphragm muscles are all significantly more damaged than C57 *mdx* muscles.

Though the exact mechanisms underlying the differences in severity between C57 *mdx* and D2 *mdx* mice remain unknown, a role for transforming growth factor β (TGF-β) has been reported. Elevated TGF-β has been previously implicated in DMD pathophysiology [106,107], and has been shown to limit myogenesis and lead to the development of muscle fibrosis [108–111]. Mazala et al. (2020) found that the D2 *mdx* mice have chronically elevated TFG-β contributing to impaired satellite cell function and excessive fibrosis [112]. However, to the best of my knowledge, the role of Ca^{2+} dysregulation in mediating differences in disease severity between *mdx* models has not been examined. Indeed, the earlier onset of soleus and EDL muscle weakness in the D2 *mdx* compared with C57 *mdx* suggests that differences in Ca^{2+} regulation may exist. Further, given the importance of Ca^{2+} regulation, particularly RyR and SERCA function in dystrophic pathology, it would be of interest to characterize their function in the D2 *mdx* mouse model. However, to my knowledge this has not yet been done. Investigating the function of RyR and SERCA in the D2 *mdx* mouse model would be the first step in determining whether Ca^{2+} dysregulation plays a role in the worsened D2 *mdx* pathology further supporting the importance of Ca^{2+} homeostasis in DMD.

Chapter 2: Thesis Aims

2.1 Statement of Research Problem

Previous studies in the C57 *mdx* have clearly demonstrated a role of RyR leak and impaired SERCA function in dystrophic pathology further demonstrating the importance of Ca^{2+} regulation. One of the most notable limitations of the C57 *mdx* mouse is that the mice present with a relatively less severe dystrophic phenotype which reduces the transferability of mechanistic and interventional findings to human DMD patients. To circumvent this limitation, the *mdx* mouse was crossed onto the DBA/2J strain giving rise to the D2 *mdx* mouse. Unlike the C57 *mdx* mice, the D2 *mdx* mice displays a more severe and earlier onset pathophysiology. Currently the exact underlying mechanisms explaining the differences in severity remain unknown. More specifically, whether the function of Ca^{2+} handling proteins RyR and SERCA are further impaired in the D2 *mdx* mouse muscles compared with the C57 *mdx* mouse remains to be investigated. This is important as it this data would provide indication as to whether SERCA and/or RyR and Ca^{2+} regulation can be targeted in the D2 *mdx* mouse.

2.2 Purpose

The purpose of this study is to determine if Ca^{2+} handling, specifically by RyR and SERCA, is further impaired in the skeletal muscles obtained from D2 *mdx* mice compared to those from the C57 *mdx* mice.

2.3 Hypotheses

The overarching goal of this thesis is to examine SR calcium regulation in the C57 and D2 *mdx* mice at an age, where D2 *mdx* mice show worsened pathology compared with C57 mdx mice (i.e., smaller and weaker muscles). Along with worsened pathology, I hypothesize SERCA-mediated calcium uptake and activity will be most impaired in the D2 *mdx* muscles. I also hypothesize that D2 *mdx* muscles will have the most SR Ca^{2+} leak, contributing to dysfunctional SR Ca^{2+} handling and weakness. Associated with these changes in SR calcium handling, particularly in the D2 *mdx* mice, will be an increase in irreversible RONS modifications and calpain activity.

Chapter 3: Methodology

3.1 Animals and Design

Male C57 *mdx* (n = 12), C57 WT (n = 12), D2 *mdx* (n = 12), and D2 WT (n = 12) mice were purchased from Jackson Laboratories at 7-8 weeks of age. They were acclimated and housed in Brock University's Animal Facility, in an environmentally controlled room with a standard 12:12 hour light-dark cycle and allowed access to food and water *ad libitum*. After the mice reached 9-10 weeks of age, they were euthanized via cervical dislocation under general anesthetic (vaporized isoflurane) and their tissues were collected. All animal procedures were reviewed and approved by the Animal Care Committee of Brock University and followed the guidelines of the Canadian Council on Animal Care (see Appendix A).

3.2 Metabolic Caging

At 7-8 weeks of age, mice were housed in pairs in a Promethion Metabolic Cage System for 48 hours. Two 12-hour light and dark cycles were measured, and data was collected. Food and water intake were measured through mass changes with the MM-1 load cell, the Promethion mass measurement device. Cage ambulation was quantified through metres travelled which is collected through beam breaks with the BXYZ Beambreak Activity Monitor in the x y, and z planes. Respiratory exchange ratio (RER) was calculated as VCO_2 (volume of carbon dioxide expired each minute) divided by VO_2 (volume of oxygen inspired each minute) measured from the Promethion metabolic cages equipped with O_2 and CO_2 gas analyzers. To obtain mean energy expenditure expressed in kcal/hr, the Weir equation was used [113].

3.3 Sample collection and homogenization

Gastrocnemius muscles (n=12/group) were rapidly extracted from euthanized animals and flash frozen in liquid N2 and stored at -80˚C. For SERCA uptake and activity analyses, muscles were homogenized in homogenizing buffer (5 mM HEPES, 250 mM sucrose, 0.2 mM PMSF, 0.2% NaN3; pH 7.5) at 10 times the weight of the muscle (muscle weight in mg * 10 = μl of homogenizing buffer). An aliquot of muscle was then supplemented with Protease (phosSTOP 04096845001)/Phosphatase (cOmplete Mini, EDTA-free 11836170001) inhibitors for western blot analyses.

3.4 Uptake + leak

Ca^{2+} uptake rate was recorded across each sample and measured with a spectrofluorometric assay and Indo-1 in the gastrocnemius muscle. Indo-1 (Cayman Chemicals # 20418) was added to each sample and was excited at 350nm. Samples were then be read at 405nm to measure Indo-1 bound to Ca^{2+} and at 485nm to measure Ca^{2+}-free Indo-1. The ratio of bound:unbound Indo-1 was used to calculate free Ca^{2+} ($[Ca^{2+}]_f$) in each sample. This assay was performed first (n=6 per group) on a Photon Technology International (PTI) spectrofluorometer (Ratiomaster system, Photon Technology International, Birmingham, NJ) equipped with dual-emission monochromators. Briefly, 150 μl of gastrocnemius homogenate was pipetted into 2 ml of uptake buffer (20mM HEPES, 200mM KCL, 10mM NaN_3, 5μM TPEN, 15mM $MgCl_2$, 5mM Oxalate; pH 7.0), constantly stirred in a 4ml cuvette, and held in a heated jacket at 37˚C. Then, 2 μl of Indo-1 was pipetted into the cuvette, followed by the addition of 40 μl of 250 mM ATP, which initiated calcium uptake. Once the uptake plateaued, 1 μl of SERCA-specific inhibitor, cyclopiazonic acid (CPA) (40mM, Sigma #239805) was added to inhibit SERCA activity,

leading to Ca^{2+} leak. Following the leak portion of the assay, each sample was calibrated using a two-point system. First, 145 μl EGTA was added to create a low-Ca^{2+} point as EGTA chelates calcium. Then, 40 μl of high Ca^{2+} (10 M $CaCl_2$) was added to the cuvette to saturate Indo-1 and create a high-Ca^{2+} calibration point. Using Formula 1 (listed below) and a dissociation constant of 250mM^{-1}, the free Ca^{2+} concentration ($[Ca^{2+}]_f$) in each sample was measured. The amount of Ca^{2+} uptake and leak was measured through an area under the curve (AUC) analysis.

$$[Ca^{2+}] = K_d \left(\frac{R - R_{min}}{R_{max} - R}\right)\left(\frac{S_{f2}}{S_{b2}}\right)$$

Formula 1: Free Calcium Concentration ($[Ca^{2+}]_f$)
K_d is the dissociation constant of Indo-1 (250nM). R_{min} refers to the ratio of bound:unbound Indo-1 in the EGTA portion. R_{max} refers to the ratio of bound:unbound Indo-1 in the high Ca^{2+} portion. S_{f2} is the fluorescence emission at 485nm (Ca^{2+}-free Indo-1) in the EGTA portion and S_{b2} is the fluorescence emission at 485nm in the high Ca^{2+} portion.

We recently fitted the Ca^{2+} uptake assay onto a 96-well plate using our M2 Molecular Device plate reader (Molecular Devices, San Jose, CA) to allow for a high-throughput analyses with less sample requirement (25 μl of sample vs 150 μl). To determine whether this 96-well plate assay would produce similar results to that observed in the PTI spectrofluorometer, another set of gastrocnemius samples (n=6) were processed. In brief, 200 μl of uptake buffer, 25 μl of gastrocnemius homogenate, and 1 μl of Indo-1 was pipetted into black Eppendorf tubes. 100 μl of this mixture was then loaded in duplicate on a black 96-well plate and read for starting Ca^{2+} levels. Swiftly, 4 μl of ATP was added to each well, and the plate was read with a kinetic program set with an excitation wavelength of 355 nM and emission wavelengths of 405 nm (Ca^{2+}-bound Indo-1) and 485 nm (Ca^{2+}-free Indo-1). After 800 seconds, the program was paused and 1 μl of CPA was added to inhibit the SERCA pump and initiate SR Ca^{2+} leak. The plate was

read for another 600 seconds. In the dithiothreitol (DTT, Bioshop #DTT001) treatment, conditions were similar, except 26 μl of DTT was added with 174 μl of uptake buffer in the sample mixture and allowed to incubate for 10 min. The amount of Ca^{2+} uptake and leak were measured through an area under the curve analysis (AUC). In addition, rates of Ca^{2+} uptake and leak were analyzed and normalized to grams of protein measured by a BCA assay.

3.5 SERCA Activity

An enzyme-linked spectrophotometric assay measuring ionophore-supported SERCA activity was measured across a range of Ca^{2+} concentrations (pCa 7.0 -5.0) on a 96-well plate. The SERCA activity assay links ATP hydrolysis to the disappearance of NADH using pyruvate kinase (PK, Sigma #P1506-25KU) and lactate dehydrogenase (LDH, Sigma #L2625-25KU) (18 U l^{-1} for both). This assay was performed on a M2 Molecular Devices MultiMode plate reader (n=6/group). Ca^{2+} ATPase buffer (20mM HEPES, 200mM KCl, 10mM NaN3, 1mM EGTA, 15mM MgCl2, 5mM ATP, 10mM phosphoenolpyruvate [Biobasic, #PB0687]) was made and stored at -20ºC prior to experimentation. A reaction master mix was made including 5 mL ATPase buffer, 12 μl LDH, 18 μl PK, 10.5 μl Ionophore (Sigma, #A23187) and 10 μl of gastrocnemius sample. Then, 300 μl of reaction master mix were added to 16 separate Eppendorf tubes, each loaded with different volumes of 10 mM $CaCl_2$ (8 μl, 9 μl, 10 μl, 10.5 μl, 11 μl, 11.5 μl, 12 μl, 13 μl, 14 μl, 15 μl, 16 μl, 17 μl, 18 μl,19 μl, 20 μl, 20 μl + 1μl of 40mM CPA) and mixed, before loading 100 μl of each tube in duplicate onto a 96-well clear plate. Next, 4 μl of 1.9% (w/v) NADH (Sigma, #45507628) was added to start the reaction. The plates were read at 340 nm for 30 minutes. SERCA activity in gastrocnemius homogenates was

calculated with a pathlength correction, extinction coefficient of NADH (6.22 mM), and the subtraction of ATPase activity in the presence of 1 μl SERCA-specific inhibitor, CPA (40 mM) from total ATPase activity across the range of calcium concentrations. The calcium concentration in each tube was measured and calculated using the fluorometric indicator, Indo-1 and reported as *p*Ca (negative logarithm of $[Ca^{2+}]$. A bicinchoninic acid (BCA) assay was done to normalize submaximal and maximal SERCA activity to grams of protein loaded into each well.

3.7 Western Blotting

Western blotting was conducted in gastrocnemius homogenates to determine protein expression of SERCA1a/2a, total and phosphorylated PLN, SLN, RyR1 and calstabin. Laemmli buffer (BioRad, Mississauga, ON) was added to muscle homogenates and electrophorectially separated at 240V for 22 minutes on a 7-12% TGX gradient gel (BioRad). Proteins were transferred to PVDF or nitrocellulose membranes for 6 minutes using BioRad Trans Blot Turbo and TGX Turbo settings, or methodology specified in Table 3.1. Prior to blocking, SuperSignal western Blot Enhancer (46641; Thermo Scientific, Mississauga, ON) was applied for SLN blot. A 5% (w/v) milk and TBST solution was used to block the membranes for one hour. Primary antibody was then added and incubated overnight at 4°C. The primary antibodies SERCA1a (MA3-911), SERCA 2a (MA3-919), calstabin (PA1-026A) were obtained from ThermoFisher Scientific (Waltham, MA, USA). The primary antibody for SLN (ABT13) was obtained from Sigma-Aldrich (Oakville, ON, CA). The primary antibody for nitrocysteine (ab94930) was obtained from Abcam (Cambridge, UK). The primary antibody for nitrotyrosine (189542) was obtained from Cayman Chemical (Ann Arbor, MI, USA). Subsequent to primary incubation, the

membranes were washed three times with TBST and then incubated with anti-mouse (SERCA1a/2a, RyR1 ;7076; Cell Signalling Technology, Whitby, ON) or anti-rabbit (calstabin, SLN; 7074, Cell Signalling Technology,) secondary antibodies at room temperature for 1 hour. The membranes were then washed again three times with TBST then chemiluminescent substrate Millipore Immobilon (WBKLS0500; Sigma-Aldrich) or SuperSignal West Femto Maximum Sensitivity Substrate (34095; Thermo Scientific) was added prior to imaging with a BioRad Chemidoc . Optical densities were analyzed with imageLab (BioRad) and normalized to total protein visualized with a ponceau stain (59803; Cell Signalling Technology).

Table 3.1: Western Blotting Conditions

	Membrane	Running Conditi-ons	Transfer Conditi-ons	Membrane	Primary Dilution	Secondary Type & Dilution	Chemilumin-escent Substrate
SERCA1a /2a	TGX Precast	22 min at 240V	6 min (TGX Turbo)	PVDF	1:2,000	Anti-mouse; 1:10,000	Immobilon
RyR1	TGX Precast	45 min at 240V	6 min turbo	PVDF	1:1,000	Anti-mouse; 1:2,000	Immobilon
Calstabin1	TGX Precast	22 min at 240V	6 min turbo	PVDF	1:1,000	Anti-rabbit; 1:5,000	Immobilon
SLN	Tricine	15 min at 100V, then 60 min at 120V	90 min wet transfer	Nitrocellulose	1:500	Anti-rabbit; 1:2,000	West Femto
Nitro-tyrosine	TGX Precast	22 min at 240V	6 min turbo	PVDF	1:2,000	Anti-mouse; 1:10,000	Immobilon
Nitro-cysteine	TGX Precast	22 min at 240V	6 min turbo	PVDF	1:2,000	Anti-mouse; 1:10,000	Immobilon

3.8 Calpain Assay

A commercialized calpain assay (QIA120; Millipore Sigma) was used in order to determine calpain activity in the gastrocnemius. Tissue was freshly homogenized in RIPA lysis buffer (632424; Millipore Sigma) at a 1:20 ratio. Using the kit, 50 μl of sample was placed in duplicate in either 100 μl of activator buffer (with 1 μl of reducing agent) or 100 μl of inhibitor buffer in a 96-well plate. Then, 50 μl of diluted substrate was added in the

dark into each well and the plate was incubated for 15 minutes. The plate was then measured for 10 minutes as a kinetic plate at an excitation of 370 nm and emission of 450 nm to determine the rate of calpain activity normalized to total protein.

3.9 Statistical Analysis

A two-way ANOVA was used to test the main effects of genotype (*mdx*) and strain (C57 or D2) and their potential interaction for most analyses. Post-hoc testing was completed using Sidak multiple comparison testing. A Student's t-test was also used to compare cage ambulation data. Statistical tests were conducted using GraphPad Prism 8 Software (San Diego, USA). All values are presented as means ± standard error. Statistical significance is set to $p \leq 0.05$.

Chapter 4: Results

4.1 Differences in Muscle and Body Mass

Body and gastrocnemius muscle mass were recorded at 10 weeks of age (Figure 1). For body mass, a significant main effect of *mdx* and strain were found, along with a significant interaction between *mdx* and strain (Figure 4.1A). Sidak's post-hoc analyses revealed that while C57 WT and C57 *mdx* had similar body mass, the D2 *mdx* mice weighed significantly less than the D2 WT mice ($p < 0.0001$, Figure 1A). A significant main effect of strain was also detected for gastrocnemius muscle mass, however, there was no effect of *mdx* nor was there an interaction when expressed in absolute and relative (to body mass) terms (Figure 1 B and C).

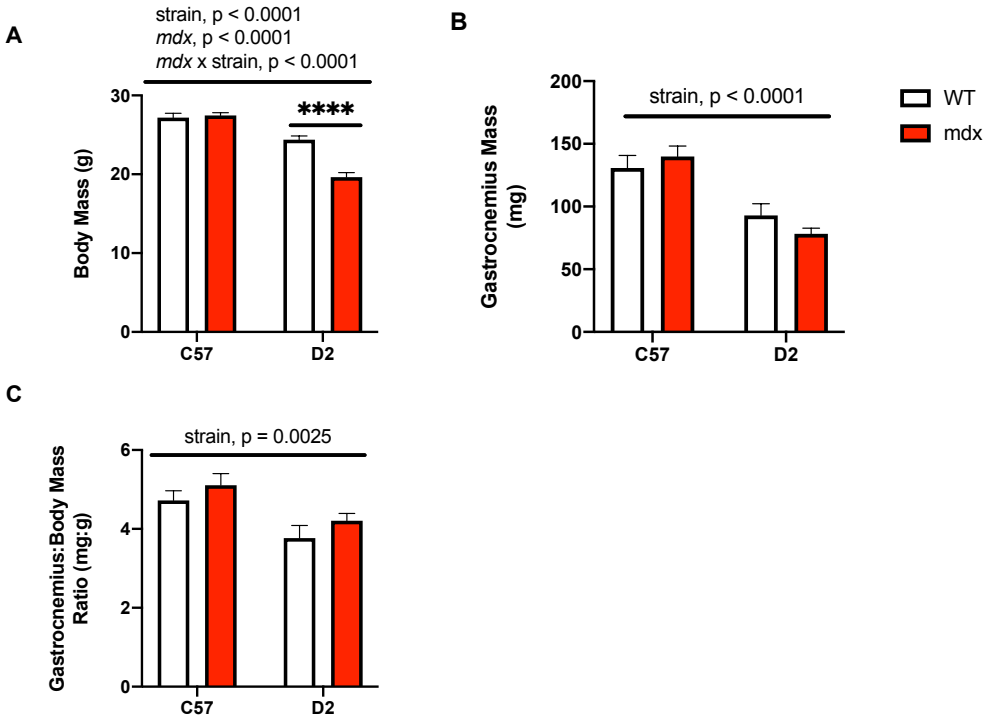

Figure 4.1: Body and muscle mass are dependent on genetic background. A) Body weight, B) gastrocnemius weight, C) gastrocnemius mass:body mass ratio (mg:g). Values are represented as mean ± SEM. A two-way ANOVA was used for all comparisons, n=12 per group. **** $p < 0.0001$ with a Sidak's post hoc test.

4.2 Cage activity and metabolic caging

Water intake, food intake, cage activity, energy expenditure and respiratory exchange ratio (RER) were measured over a 48-hour period. Light and dark cycles (12-hours each) were analyzed along with a daily 24-hour period. Two-way ANOVA of water intake revealed that there was a significant main effect of background strain (D2 vs. C57) in the light cycle and daily 24-hour period (Figure 4.2 A and C). We did not detect a main effect of *mdx* genotype or an interaction between strain and *mdx* genotype across any time period (Fig. 4.2 A-C).

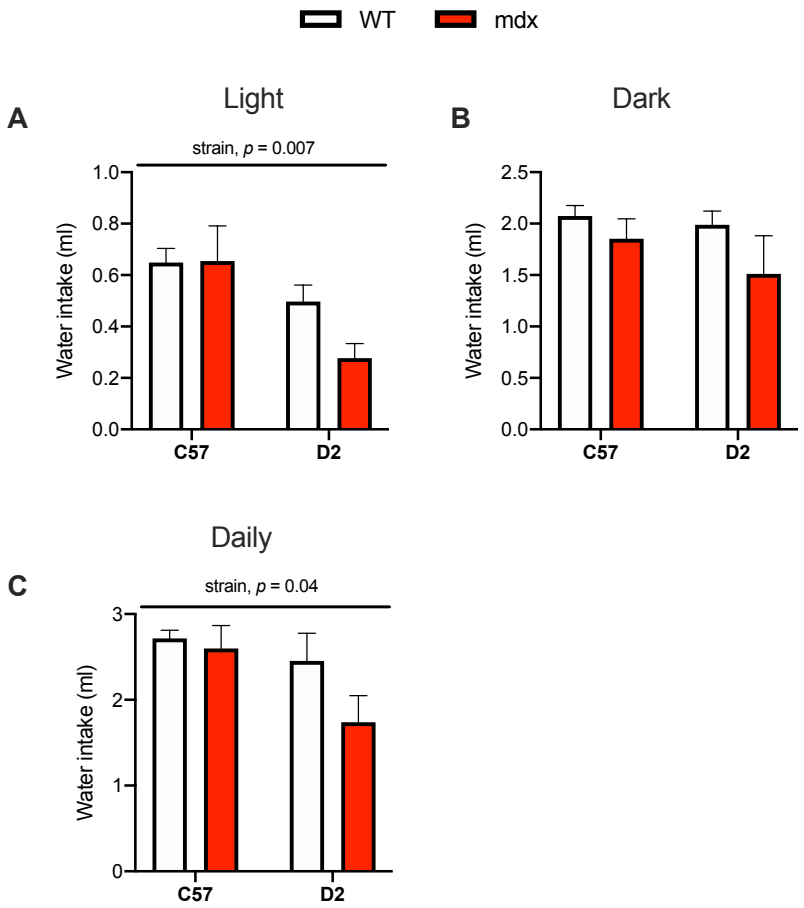

Figure 4.2: Water Intake. Water intake was measured in A) light (12-hr), and B) dark cycles (12-hr), as well as during a C) daily 24-hour period. Values are represented as mean ± SEM. Main effects expressed in bars over the graph. A two-way ANOVA was used for all comparisons, n=5-6 per group.

Food intake was analyzed in a similar fashion. Two-way ANOVA analysis of food intake revealed a significant main effect of background strain in the light, dark, and daily time periods (Figure 4.3 A-C). A significant main effect of *mdx* was found in the dark and daily time periods (Figure 4.3 B and C). A significant interaction between *mdx* and background strain was detected in the dark period, with post-hoc analyses showing that only the D2 *mdx* mice had significantly reduced food intake vs their respective WT.

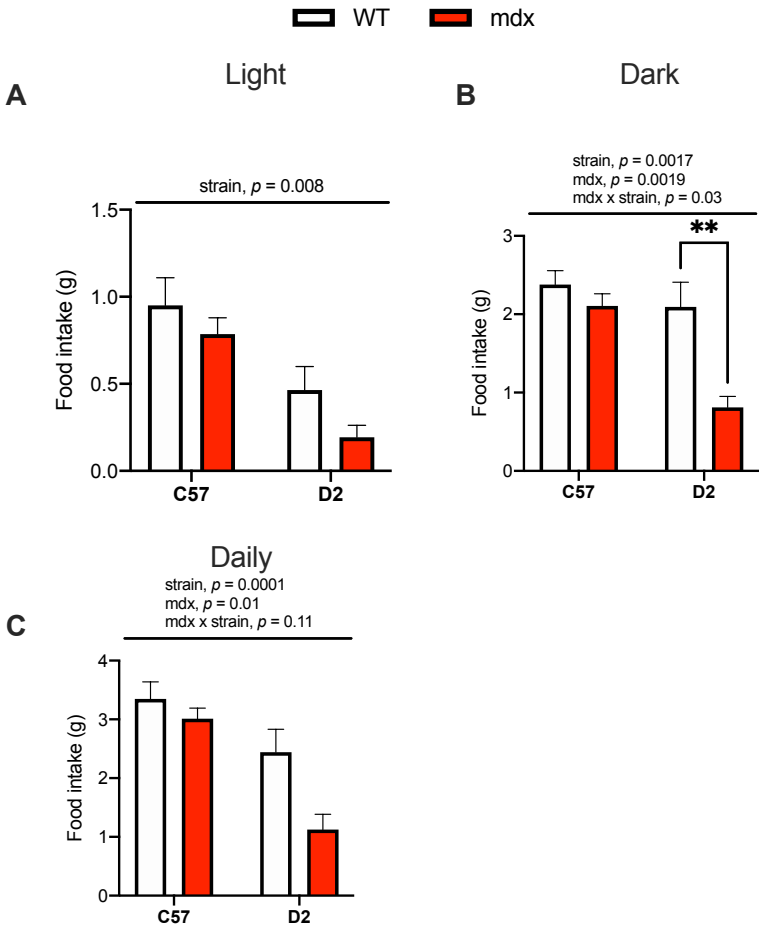

Figure 4.3: Food Intake. Food intake was measured in A) light (12-hr), and B) dark cycles (12-hr), as well as during a C) daily 24-hour period. Values are represented as mean ± SEM. Main effects expressed in bars over the graph. A two-way ANOVA was used for all comparisons, n=5-6 per group. $^{**}p < 0.01$ with a Sidak's post hoc test.

Cage ambulation quantified the amount of physical movement (in meters travelled) the mice had while housed in the metabolic cages not including fine movements like grooming. Two-way ANOVA revealed a significant main effect of strain throughout the light, dark and daily periods showing that D2 mice were less ambulant in their cages compared with C57 mice, irrespective of the WT or *mdx* genotype (Figure 4.4 A-C). There was no main effect of *mdx* or interaction between *mdx* genotype and background strain detected. However, it is important to note that since the main effect of strain was so prominent, accounting for 40-60% of total variation in the data, detecting a main effect of *mdx* or an interaction would be difficult. Indeed, a Student's t-test showed that D2 *mdx* mice are less ambulant in their cages compared with D2 WT mice across the light (p = 0.04), dark (p = 0.004), and daily 24-hour (p = 0.06) time periods. However, this was not observed when comparing C57 *mdx* and C57 WT mice (p = 0.65 – 0.95).

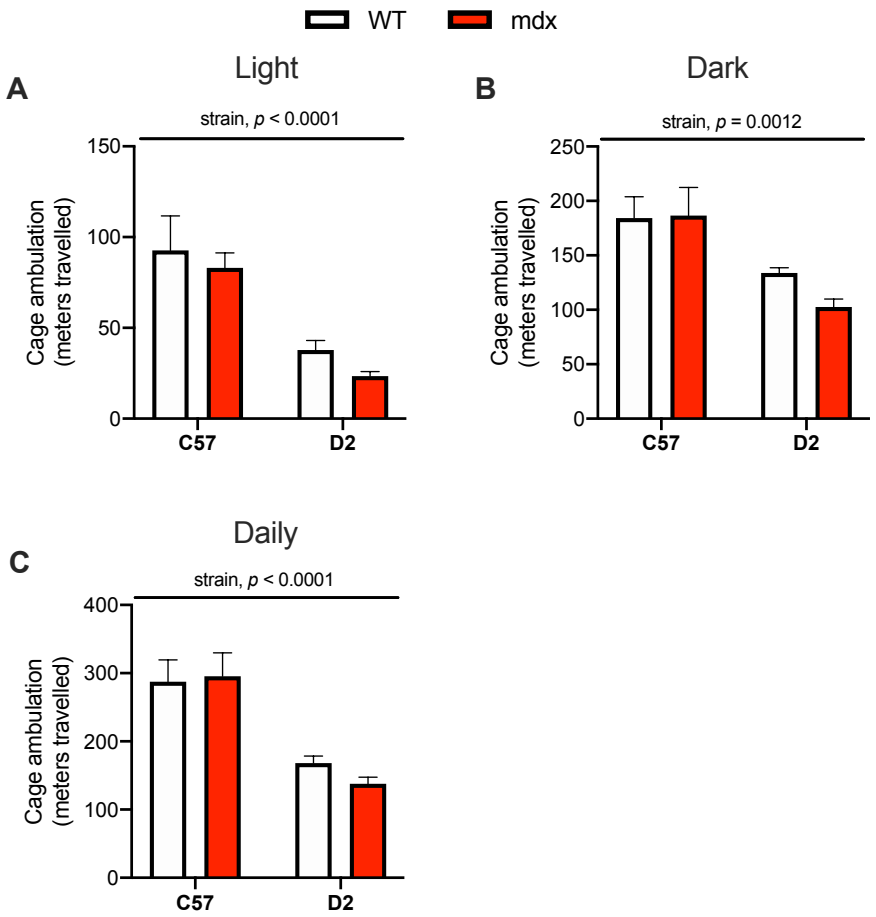

Figure 4.4: Cage Ambulation. Cage ambulation was measured in A) light (12-hr), and B) dark cycles (12-hr), as well as during a C) daily 24-hour period. Values are represented as mean ± SEM. Main effects expressed in bars over the graph. A two-way ANOVA was used for all comparisons, n=5-6 per group.

Energy Expenditure

Using indirect calorimetry and the Weir equation, energy expenditure was measured then normalized to body mass (kg). Two-way ANOVA analysis showed a significant interaction between the *mdx* genotype and background strain in all time periods (Figure 4.5 A-C). Sidak post-hoc analysis showed that D2 *mdx* mice had significantly greater energy expenditure compared to D2 WT mice whereas there were no differences between C57 *mdx* and C57 WT mice (Figure 4.5 A-C).

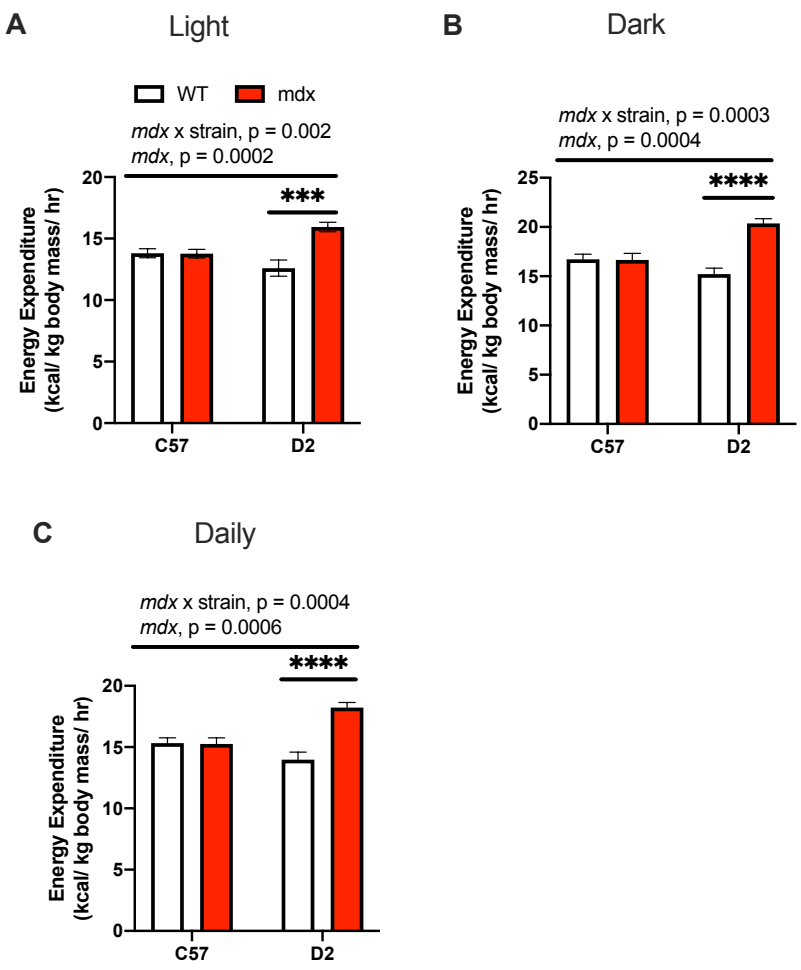

Figure 4.5: Energy Expenditure. Relative energy expenditure was measured in A) light (12-hr), and B) dark cycles (12-hr), as well as during a C) daily 24-hour period. Values are represented as mean ± SEM. Main effects expressed in bars over the graph. A two-way ANOVA was used for all comparisons, n=5-6 per group. ***$p < 0.001$, ****$p < 0.0001$ with a Sidak's post hoc test.

Respiratory Exchange Ratio

Respiratory exchange ratio (RER) was calculated as VCO_2 expelled over VO_2 consumed. Two-way ANOVA analysis showed interaction effects between *mdx* and strain in the dark and daily time periods with no effects observed during the light cycle (Figure 4.6 A-C).

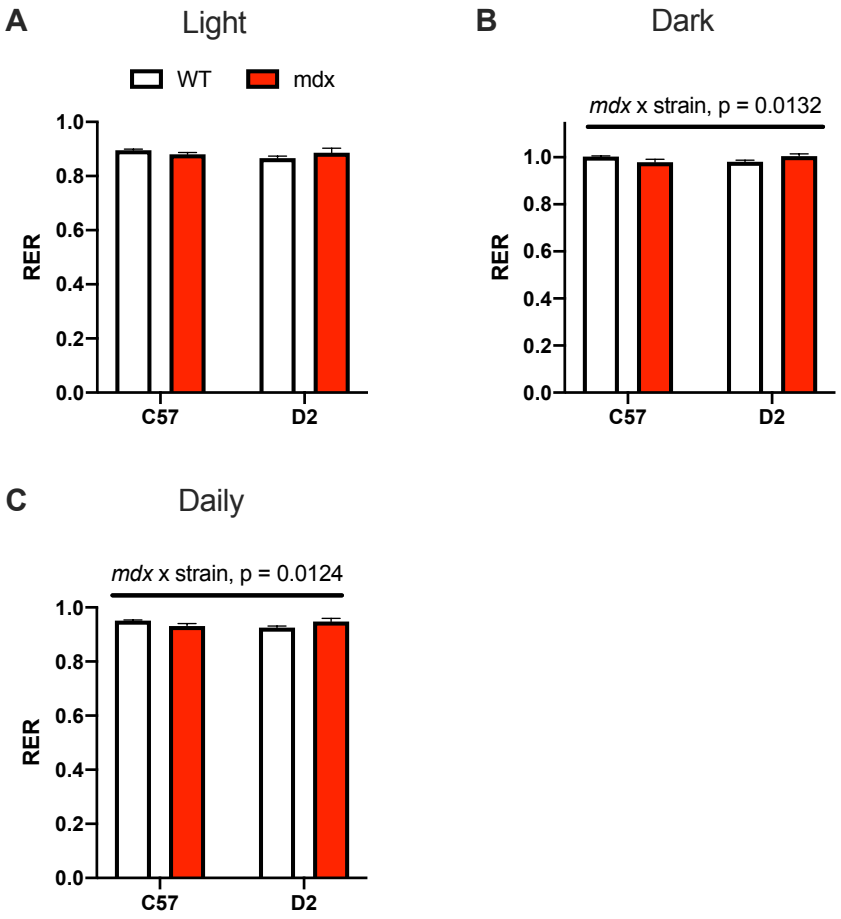

Figure 4.6: Respiratory Exchange Ratio. Respiratory exchange ratio was measured in A) light (12-hr), and B) dark cycles (12-hr), as well as during a C) daily 24-hour period. Values are represented as mean ± SEM. Main effects expressed in bars over the graph. A two-way ANOVA was used for all comparisons, n=5-6 per group.

4.2 SR Calcium Uptake and Leak

PTI 2 mL cuvette assay

SERCA-mediated Ca^{2+} uptake and leak were measured in gastrocnemius homogenates in a 2 mL cuvette assay using the membrane-impermeable Ca^{2+} fluorometric dye, Indo-1 (Figure. 4.7 and 4.8). When the samples are given ATP, SERCA uses this energy to catalyze Ca^{2+} transport into the SR, causing dissociation from Indo-1 in the cytoplasm and dropping $[Ca^{2+}]_{free}$ over time (Figure 4.7A). While this can be seen occurring similarly in the C57 WT, D2 WT and C57 *mdx* samples, the D2 *mdx* samples start at a higher $[Ca^{2+}]_{free}$ and are less able to drop $[Ca^{2+}]_{free}$ over time (Figure 4.7A). In statistical support of this, two-way ANOVA analyses of the area under the curve (AUC) revealed a significant interaction effect between background strain and mdx genotype, with a Sidak's post-hoc test showing a significant increase in AUC in the D2 *mdx* gastrocnemius compared to the D2 WT (Figure 4.7B). Similarly, analyses of starting $[Ca^{2+}]_{free}$ revealed a trending ($p = 0.06$) interaction between background strain and mdx genotype, where the D2 *mdx* muscles appear to have a higher starting $[Ca^{2+}]_{free}$ compared with WT (Figure 4.7C). As AUC, is inherently affected by the starting $[Ca^{2+}]_{free}$, data was then made relative to starting $[Ca^{2+}]_{free}$ (Figure 4.7D). Despite this normalization, uptake was still visibly impaired in the D2 *mdx* gastrocnemius muscles. Further, relative AUC analyses revealed a significant interaction between *mdx* genotype and background strain, with a Sidak's post-hoc test showing a significantly greater AUC in D2 *mdx* samples compared to D2 WT sample, and yet no differences in C57 *mdx* and C57 WT mice (Figure. 4.7E).

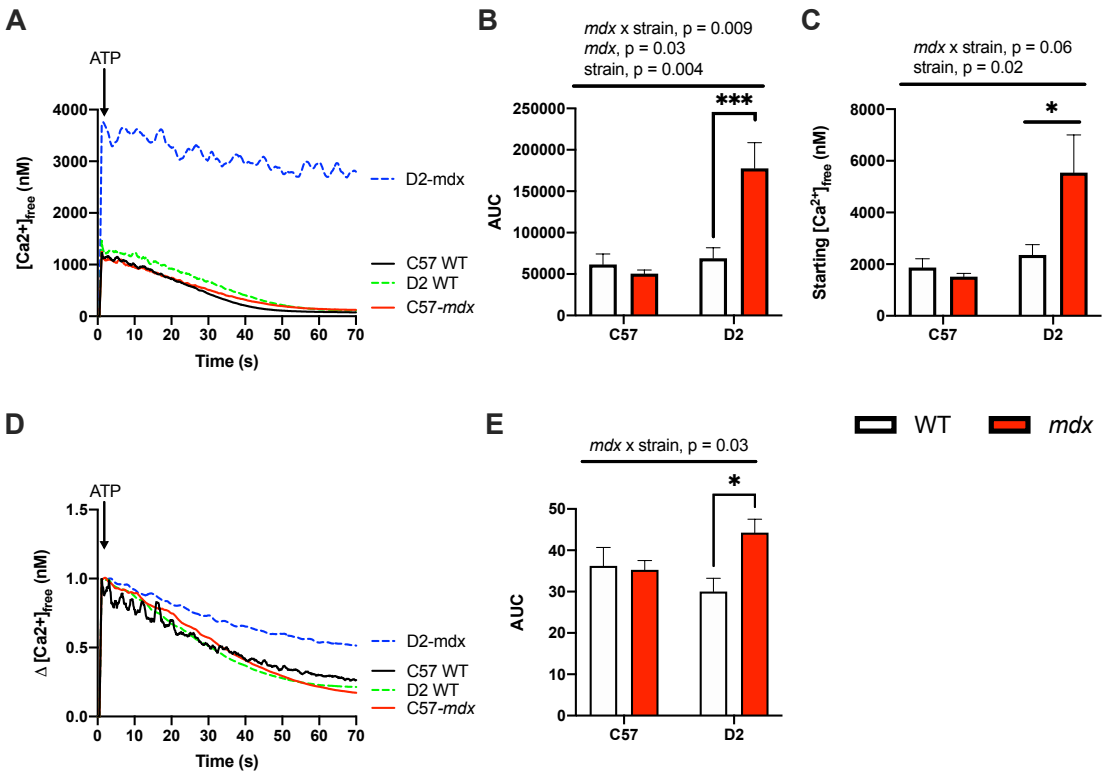

Figure 4.7: Gastrocnemius Ca^{2+} uptake assay (2mL cuvette). A) Ca^{2+} tracing of absolute uptake in gastrocnemius homogenates. B) Area under the curve of absolute Ca^{2+} uptake. C) Starting Ca^{2+} levels immediately after ATP addition. D) Calcium tracing of uptake relative to starting calcium. E) Area under the curve of relative Ca^{2+} uptake. Values are represented as mean ± SEM. Interaction and main effects expressed in bars over the graph. Significance is indicated by $*p < 0.05$, $**p < 0.01$, $***p < 0.001$, with a two-way ANOVA along with a Sidak's post hoc test, n =5-6 per group.

After allowing SERCA Ca^{2+} uptake to plateau, SR Ca^{2+} leak was initiated with the addition of CPA, which inhibits the SERCA pump. Upon CPA addition, $[Ca^{2+}]_{free}$ rises as Ca^{2+} is released back into the cytoplasm (Figure 4.8). There was a similar leak pattern/trace between C57 WT, D2 WT and C57 *mdx* samples, however, SR Ca^{2+} leak was dramatically lower in the D2 *mdx* gastrocnemius samples (Figure 4.8 A). AUC analyses via Two-way ANOVA revealed a trending interaction between background strain and the *mdx* genotype ($p = 0.06$), where the D2 *mdx* mice appeared to have less Ca^{2+} leak (lower AUC) compared with WT.

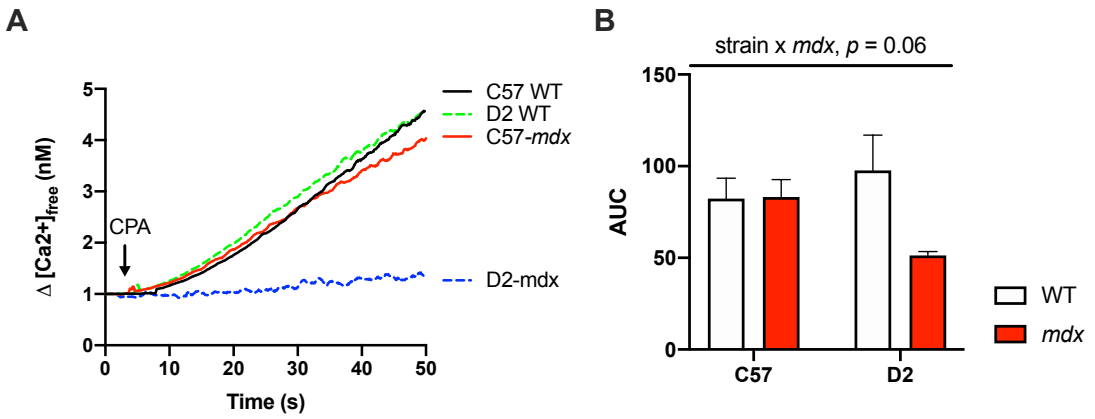

Figure 4.8: Gastrocnemius Ca^{2+} leak (2 mL cuvette). SR Ca^{2+} leak was measured after reaching the plateau of Ca^{2+} uptake in gastrocnemius homogenates. A) Depicts the change in $[Ca^{2+}]_{free}$ relative to starting $[Ca^{2+}]$ prior to the addition of cyclopiazonic acid (CPA). The addition of CPA inhibits the SERCA pump allowing for SR Ca^{2+} to be released back into the cytosol. B) Area under the curve analysis. Values are represented as mean ± SEM. For B) a two-way ANOVA was used.

Molecular Devices 96-well plate reader assay

While this thesis was underway, the Ca^{2+} uptake assay was fitted onto a 96-well plate to circumvent technical and analytical limitations associated with the 2 mL cuvette assay (see discussion). Thus, in a separate set of 6 mice per group, Ca^{2+} uptake and leak experiments were repeated. Figure 4.9 reveals similar results of Ca^{2+} uptake with an obvious impairment in D2 *mdx* gastrocnemius samples and higher starting Ca^{2+} concentration (Figure 4.9 A and B). AUC analyses also produced similar findings, with a significant main effect of *mdx* genotype and a significant interaction between background strain and *mdx* genotype (Figure 4.9 C). A Sidak's post-hoc analyses revealed that only the D2 *mdx* muscles had significantly higher AUC, demonstrating impaired Ca^{2+} uptake compared with D2 WT (Figure 4.9 C). Furthermore, even after expressing the data relative to starting $[Ca^{2+}]_{free}$ to account for the differences observed in Figure 4.9B, a significant interaction between *mdx* genotype and background strain was observed indicating that the D2 *mdx* mice had greater AUC compared with D2 WT and thus less Ca^{2+} uptake (Figure 4.9 C and D).

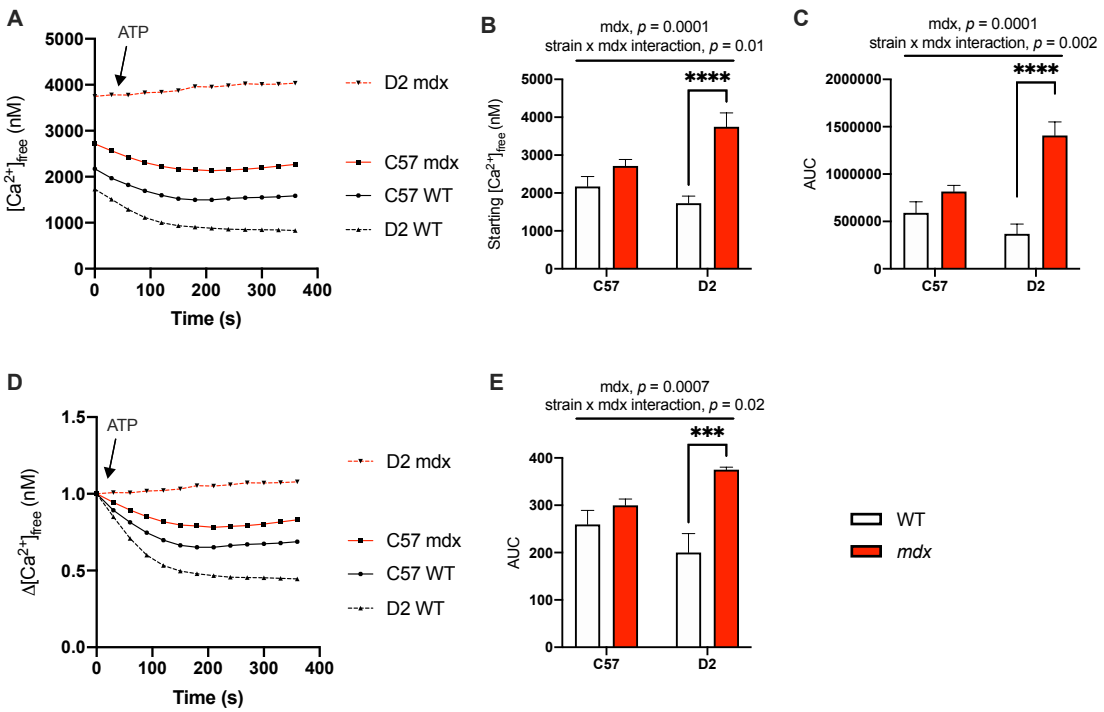

Figure 4.9: Gastrocnemius Ca^{2+} uptake (96-well plate reader assay). A) Calcium tracing of absolute uptake in gastrocnemius homogenates. B) Starting $[Ca^{2+}]_{free}$ levels immediately after ATP addition. C) Area under the curve of absolute Ca^{2+} uptake. D) Calcium tracing of uptake relative to starting Ca^{2+}. E) Area under the curve of relative Ca^{2+} uptake. Values are represented as mean ± SEM. Interaction and main effects expressed in bars over the graph. Significance is indicated by $*p < 0.05$, $**p < 0.01$, $***p < 0.001$, with a two-way ANOVA along with a Sidak's post hoc test, n =5-6 per group.

Once Ca^{2+} uptake reached its plateau, SR Ca^{2+} leak was initiated by adding CPA to each well (Figure 4.10). The Ca^{2+} leak traces showed that the D2 WT gastrocnemius samples had the highest amount of SR Ca^{2+} leak, followed by C57 WT, C57 *mdx* and D2 *mdx* (highest to lowest) (Figure 4.10 A). AUC analyses via Two-way ANOVA revealed a significant main effect of background strain, *mdx* genotype, and their interaction, with a Sidak's post-hoc test showing that the D2 *mdx* leak was significantly lower compared with D2 WT, with no differences in the C57 mice (Figure 4.10 B).

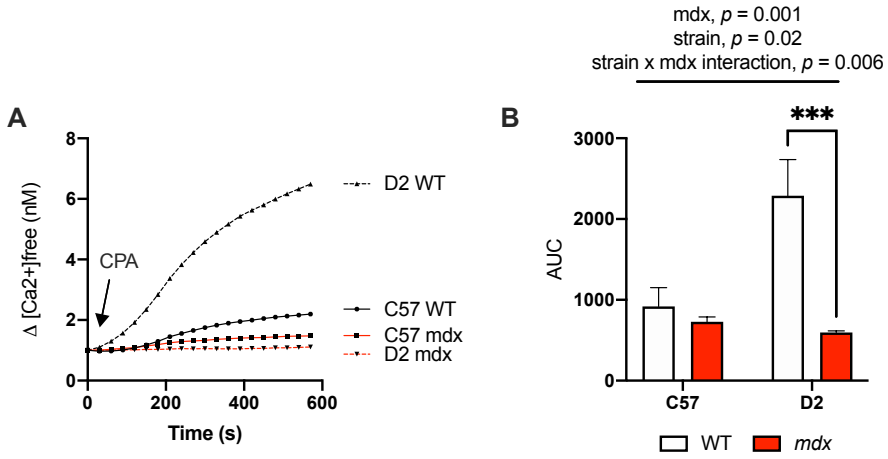

Figure 4.10: Gastrocnemius Ca^{2+} leak (96-well plate reader assay). SR Ca^{2+} leak was measured in gastrocnemius homogenates after reaching the plateau of Ca^{2+} uptake. A) Depicts the change in $[Ca^{2+}]_{free}$ relative to starting $[Ca^{2+}]$ prior to the addition of cyclopiazonic acid (CPA). The addition of CPA inhibits the SERCA pump allowing for SR Ca^{2+} to be released back into the cytosol. B) Area under the curve analysis. Values are represented as mean ± SEM. For B) a two-way ANOVA was used along with a Sidak's post hoc test, ***$p < 0.01$, n =5-6 per group.

4.3 SERCA Activity

In addition, to Ca^{2+} uptake and leak, maximal and sub-maximal rates of SERCA ATP hydrolysis were measured using a Ca^{2+}-dependent enzyme-linked spectrophotometric assay. Two-way ANOVA analysis of SERCA activity in the D2 WT and D2 *mdx* gastrocnemius muscles revealed a significant main effect of *p*Ca, highlighting the Ca^{2+} dependency of this assay, with SERCA activity increasing with elevated $[Ca^{2+}]$ (lower *p*Ca) (Figure 4.11 A). A significant main effect of *mdx* genotype was also observed suggesting lower submaximal and maximal SERCA activity in the D2 *mdx* gastrocnemius compared with D2 WT (Figure 4.11 B). When analyzing the C57 WT and C57 *mdx* data, we found a significant main effect of *p*Ca and genotype (Figure 4.11 B), which was indicative of elevated SERCA ATP hydrolysis rates in the C57 *mdx* compared with C57 WT.

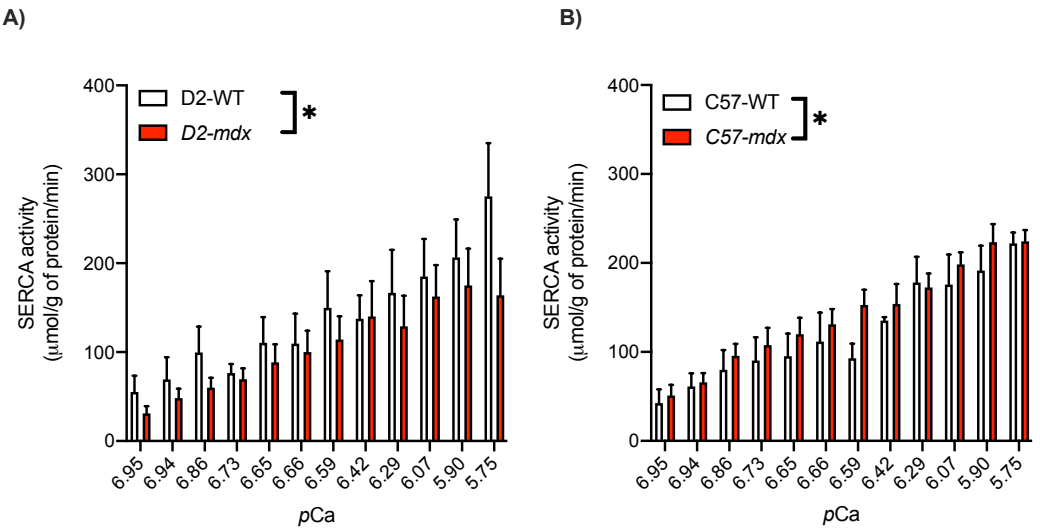

Figure 4.11: SERCA ATPase activity in gastrocnemius muscle. A) & B) SERCA ATP hydrolysis activity over varying Ca^{2+} concentrations in the D2 and C57 strains, respectively. Values are represented as mean ± SEM. A two-way ANOVA was used along with a Sidak's post hoc test * $p < 0.05$, n=6 per group.

4.4 Western Blot Analyses

In figures 4.12 and 4.13, protein contents of SR leak-related proteins were semi-quantified via western blotting in the gastrocnemius muscle. Figure 4.12 shows the total protein contents of SERCA isoforms 1a and 2a in the gastrocnemius. Two-way ANOVA analyses of SERCA1a content revealed a main effect of *mdx* genotype (Figure 4.12 A). Similarly, SERCA2a analyses revealed a significacnt main effect of *mdx* genotype, along with a significant main effect of background strain and a significant interaction between the two (Figure 4.12 B). A Sidak's post-hoc test revealed a significantly higher SERCA2a content in the D2 *mdx* samples compared to D2-WT, while this effect was not apparent in the C57 counterparts (Figure 4.12 B).

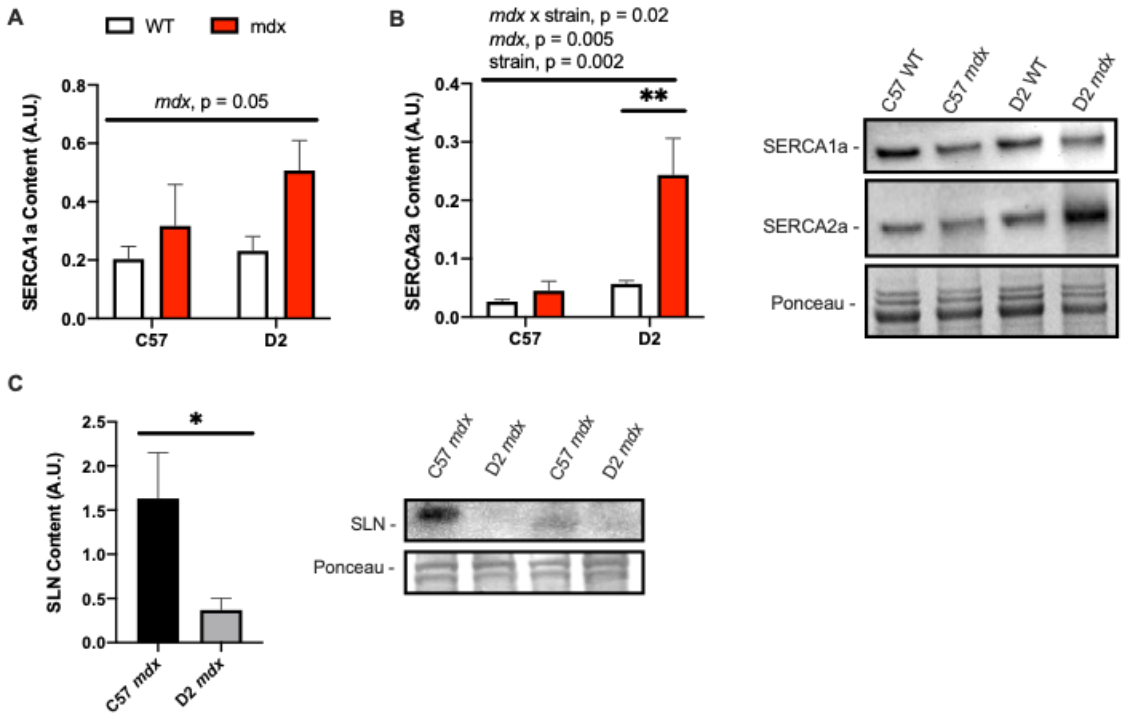

Figure 4.12: Total Protein Content of SERCA1a and SERCA2a in Gastrocnemius Muscles. SERCA1a (A), SERCA2a (B) and SLN (C) content was quantified (normalized to total protein) and expressed as arbitrary units (AU). Values are represented as mean ± SEM. A two-way ANOVA was used with a Sidak's post-hoc test (A & B), or Students' t-test (C) $*p < 0.05$, $**p < 0.01$ *mdx* vs WT per genetic strain, n= 6.

Two-way ANOVA of total RyR1 revealed main effects of *mdx* and strain (trending), while no significant differences were seen in calstabin content between mice (Figure 4.13 A and B). However, when calstabin content was expressed as a ratio with RyR1 content, a significant interaction between *mdx* and background strain was observed, with Sidak's post-hoc test showing greater calstabin: RyR1 ratio in the D2 *mdx* gastrocnemius compared to the D2 WT ($p < 0.0001$), while this difference did not exist in the C57 counterparts (Figure 4.12 C).

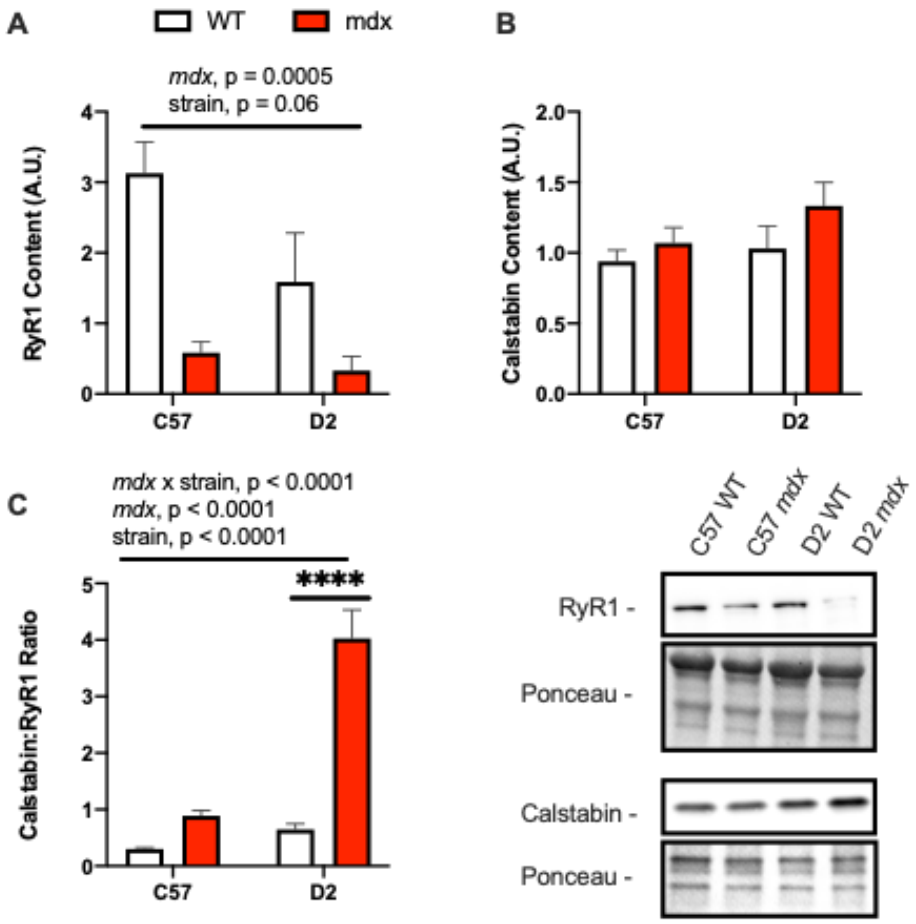

Figure 4.12: Total protein content of RyR1 and calstabin1 in gastrocnemius muscle. RyR1 (A) and calstabin (B) content was quantified (normalized to total protein) and expressed as arbitrary units (AU). C) Ratio of castabin1 over RyR1 content in gastrocnemius. Values are represented as mean ± SEM. A two-way ANOVA was used with a Sidak's post-hoc test, ****$p < 0.0001$ mdx vs WT per genetic strain, n= 6.

Figure 4.13 shows analysis of total protein tyrosine nitration and cysteine nitrosylation in the gastrocnemius. Two-way ANOVA analysis of nitrotyrosine and nitrocysteine both revealed significant main effects of *mdx*, background strain, and their interaction, albeit the interaction was only trending for nitrocysteine (Figure 4.13 A and B). Sidak post-hoc test showed that D2 *mdx* had significantly greater protein nitration and nitrosylation compared with D2 WT samples (tyrosine, $p = 0.0007$; cysteine, $p = 0.007$), whereas no differences were found in the C57 counterparts.

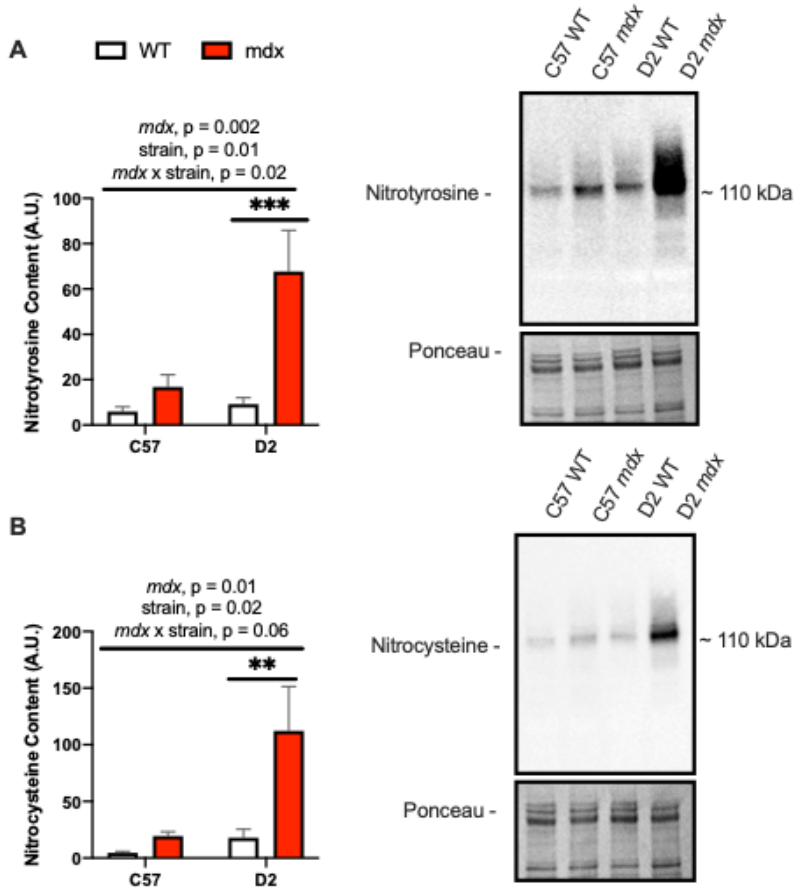

Figure 4.13: Total Nitration Content in Gastrocnemius Muscles. Protein nitrotyrosine (A) and protein nitrocysteine (B) content was quantified (normalized to total protein) and expressed as arbitrary units (AU). Values are represented as mean ± SEM. A two-way ANOVA was used with a Sidak's post-hoc test, $^{**}p < 0.01$ and $^{***}p < 0.001$ mdx vs WT per genetic strain, n= 6.

4.5 Calcium Uptake in Reducing Conditions

The results presented in Figure 4.13 show that the D2 *mdx* mice have greater levels of RONS-mediated protein modifications. As these were measured in reducing conditions (i.e., standard SDS-PAGE) these effects are likely reflective of irreversible post-translational modifications. In support of this irreversible and damaging post-translational modification, D2 *mdx* gastrocnemius homogenates were treated with DTT, a potent reducing agent, prior to loading onto a 96-well Ca^{2+} uptake assay; however, DTT treatment did not restore Ca^{2+} uptake (Figure 4.14).

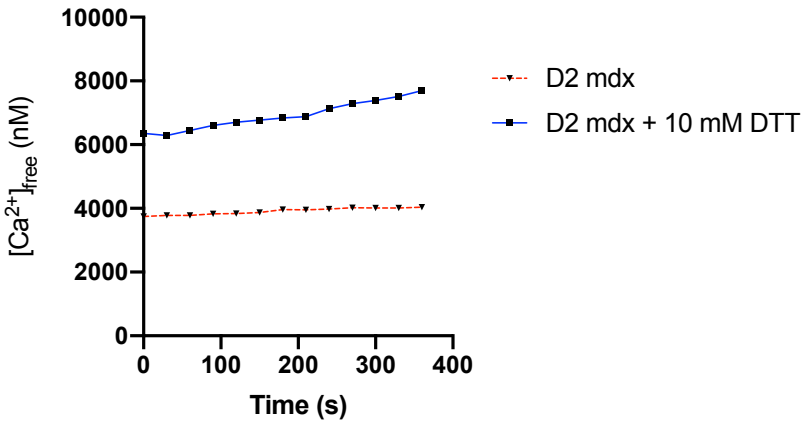

Figure 4.13: Ca^{2+} uptake non- and DTT treated of D2 *mdx* gastrocnemius homogenates. SR Ca^{2+} uptake in the D2 *mdx* gastrocnemius and D2 *mdx* treated with 10mM DTT.

4.6 Calpain Activity

A calpain activity assay was used to measure the activity of Ca^{2+}-activated cysteine proteases, which contribute to myofibril degradation and necrosis. Two-way ANOVA analysis found a main effect of *mdx* and strain (Figure 4.14). Planned comparisons also revealed a significant difference in calpain activity in D2 *mdx* vs C57 *mdx* mice ($p = 0.0006$, Student's t-test).

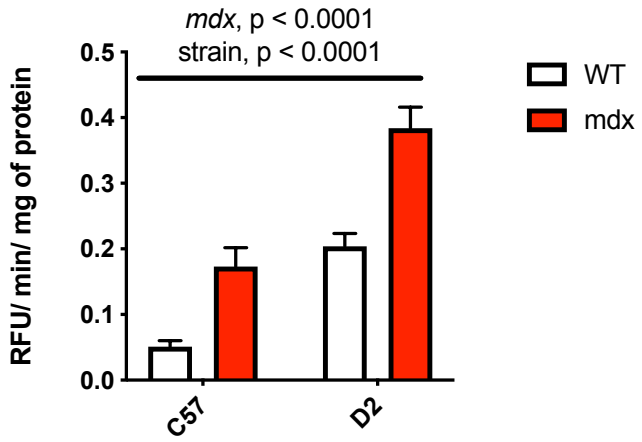

Figure 4.14: Calpain activity in the gastrocnemius homogenates. Calpain activity was measured over a 10-minute period to determine rate of activity. Values are represented as mean ± SEM. a two-way ANOVA was used and main effects expressed in bars over the graph.

Chapter 5: Discussion

The purpose of this study was to characterize SR Ca^{2+} handling in the C57 *mdx* and D2 *mdx* mice, hypothesizing that Ca^{2+} handling would be worse off in comparison in the D2 *mdx* mouse. The further decrements in Ca^{2+} handling in the D2 *mdx* mouse would likely be due to the more severe pathology displayed, which occurs at a much earlier age. In this study we sought to confirm the earlier onset of pathology in the D2 *mdx* mice compared with C57 *mdx* mice prior to examining SR Ca^{2+} handling in the gastrocnemius muscle. Notably, this is the first study to compare SR Ca^{2+} uptake and leak, in any muscular tissue in the C57 and D2 *mdx* mice.

Consistent with previous studies [101,102,105], the D2 *mdx* mice in the current study displayed smaller body mass and muscle mass; however, these differences appear to be strain specific differences between the C57 and D2 backgrounds, irrespective of the *mdx* genotype. The smaller body mass coincides with reductions in food and water intake in the D2 *mdx* mice, yet still an increase in total daily energy expenditure – highlighting a hypermetabolic state or potential net negative state. With the use of Promethion metabolic cages, we also examined daily cage activity as a marker of muscle weakness. We observed a strong main effect of background strain – where both D2 WT and D2 *mdx* mice were less ambulant in their cages. This strain main effect accounted for 40-60% of the variation in the two-way ANOVA test, likely reducing statistical power of detecting a significant interaction. Nevertheless, our planned comparisons with independent t-tests revealed that D2 *mdx* mice were less ambulant in their cages compared to D2 WT mice across all time periods analyzed, however this was not observed in C57 mice. Altogether, this suggests that at this age (10-12 weeks) only the D2 *mdx* mice are weaker than their WT counterparts. This result is consistent with previous reports showing a more severe dystrophic pathology in D2 *mdx* mice occurring at an early age [102,105].

The lower ambulation observed with the DBA/2J background may also be perpetuating the DMD phenotype in the D2 *mdx* mice as we know that low intensity exercise can combat the DMD phenotype through the activation of multiple pathways, including the calcineurin and AMP-activated protein kinase (AMPK) pathways, which enhance the oxidative gene programming [114]. Elevation of intracellular Ca^{2+} causes calcineurin to dephosphorylate transcription factor nuclear factor of activated T cells (NFAT) to active it and control the expression of multiple genes [115]. AMPK is known to enhance oxidative properties in muscle through the activation of nuclear respiratory factor-1 (NRF1), promoting mitochondrial biogenesis [116]. The promotion of the slow oxidative phenotype is a well-known mitigator of dystrophic pathology as it increases PGC-1α and utrophin content in the *mdx* mouse [117–119]. This is interesting, since additional measures of RER with the Promethion metabolic cages revealed a cross-over interaction effect, where C57 *mdx* mice had a lower RER compared to C57 WT, while D2 *mdx* had a higher RER compared to D2 WT. A lower RER correlates to a greater substrate utilization of fats or proteins as a source of energy, while a higher ratio correlates to carbohydrates as a source [120]. However, the shift towards glycolytic metabolism may be less indicative of a fibre type change and may be more reflective of substrate availability. That is, the higher reliance on carbohydrates for energy would likely correspond with large reductions in adipose tissue in the D2 *mdx* mice. In fact, body composition analysis via DXA scanning from a separate cohort of mice shows that D2 *mdx* mice have a drastic reduction in fat mass compared with D2 WT mice, outweighing the reduction in lean mass (Appendix C). Unfortunately, we obtained the InSiGHT Small Animal DXA scanner after the completion of this study, and therefore we do not have any body composition analyses for C57 *mdx* mice. The loss of fat mass may speak to further complications in these mice such as

lipodystrophy, contributing to a reduction in ability to store long-term energy sources [121]. The hypermetabolic demand we saw in the D2 *mdx* mice would likely be a partial contributor to these results also. Interestingly, Strakova et al (2018) showed that C57 *mdx* mice also have reduced body fat % and elevated RER [122]. However, this study utilized ~5-month-old mice, which could explain the discrepancy between the findings presented within this thesis. That is, the metabolic effects of dystrophin deletion may be more apparent in older C57 *mdx* mice, which would be consistent with the D2 *mdx* mice showing a more severe phenotype at an earlier onset.

To examine SR Ca^{2+} regulation, a Ca^{2+} uptake and leak assay was performed. The assay was conducted twice with two separate cohorts of n=6 per group. The first set was run using a 2 mL cuvette assay, the second using a 100 μl 96-well fitted assay. The 2 mL assay has been the long-standing Ca^{2+} uptake and leak experiment used in our lab and other labs (Professor Russell Tupling, University of Waterloo). This assay however has technical limitations. First, a large amount of required sample, which was ~150 μl of homogenate for the gastrocnemius data, negated the possibility of running samples in duplicate or triplicate. Aged Microsoft Windows software (Windows 95) led to time consuming set-up and frequent software related error codes. The rig used for the assay itself was aged and had mechanical issues including the constant deviation of the stir bar, issues warming the cuvette to 37ºC which required constant cleaning on the lines and leak in the jacket to keep the cuvette warmed to 37ºC. The Ca^{2+} tracing outputs also had a poor signal: noise ratio, making reading/analyzing data difficult. The development of the 96-well fitted assay resolved the above issues, allowing us to obtain data/outputs more reliably, as well as allowing us to measure in duplicate – giving way to greater precision.

Importantly, both assays were completed on two different cohorts, and produced very similar results, indicative of a replicable finding of impaired SERCA-mediated Ca^{2+} uptake and SR filling in the D2 *mdx* mice. Both assays communicate that firstly, the D2 *mdx* mice had a high starting myoplasmic Ca^{2+} level, which indicates impaired SR Ca^{2+} handling and could be reflective of the Ca^{2+} overload in the D2 *mdx* model. As muscles are homogenized, the internal Ca^{2+} stores are released and the SERCA pumps must act to restore resting levels. Thus, the higher levels of starting myoplasmic Ca^{2+} in the D2 *mdx* muscles are already indicative of impaired SR Ca^{2+} handling. Moreover, when the samples are provided with ATP, the Ca^{2+} decay was obviously impaired in the D2 *mdx* muscles from both samples presented in absolute or relative terms. This led to significantly higher AUC, suggesting that myoplasmic Ca^{2+} was higher in the D2 *mdx* samples throughout the uptake protocol, and that SR Ca^{2+} filling was disrupted. Further evidence of this was found when CPA was added to the reaction mixture to inhibit SERCA and to elicit SR Ca^{2+} leak. That is, the D2 *mdx* mice had the lowest amount of Ca^{2+} released back into the myoplasm with CPA addition. It is important to note that this may not suggest that RyR leak of Ca^{2+} was impaired in the D2 *mdx* mice. This is because the leak assay inherently relies on the amount of SR Ca^{2+} filling, which we know was severely impaired in the D2 *mdx* samples. However, impaired SR Ca^{2+} filling can occur through two pathways: 1) a reduction in SERCA activity and 2) enhanced leak of Ca^{2+} through RyR1. Due to a reliance of SR Ca^{2+} filling of our Ca^{2+} uptake and leak assay, we cannot determine the nature of the leak in these samples. If the samples do not have much uptake and/or a large amount of leak, the protocol would not show much leak upon the addition of CPA, as the SR does not have adequate Ca^{2+} stored. Therefore, while our assay determined that SERCA uptake is impaired, it is still possible SR Ca^{2+} leak is enhanced. Use of an assay that is less

dependent on SR Ca^{2+} filling should be used to better determine SR Ca^{2+} leak in D2 *mdx* mice.

To further compliment the SR Ca^{2+} uptake and leak results, a SERCA activity assay, which measures the rate of ATP hydrolysis, was performed. Results showed a main effect indicating that across submaximal and maximal Ca^{2+} concentrations, SERCA activity was significantly reduced in the D2 *mdx* mice compared to the D2 WT mice. Conversely, in the C57 mice, SERCA activity was elevated in the C57 *mdx* mice compared to the C57 WT mice gastrocnemius. When combined with the Ca^{2+} uptake data, the unaltered Ca^{2+} uptake with elevated ATP hydrolysis in the C57 *mdx* muscles suggests reduced SERCA transport efficiency – requiring more energy to transport Ca^{2+} into the SR. This could be due to the elevation of SLN, which is a known SERCA uncoupler that is upregulated in *mdx* muscles. SLN upregulation in dystrophic muscles coincides with disease severity, with its expression being more elevated in the *mdx*:utr knockout mice compared with *mdx* mice [84]. However, in the present study SLN was found to be elevated in both D2 and C57 *mdx* showing ectopic expression in gastrocnemius muscles, however SLN content was higher in the C57 *mdx* muscle vs D2 *mdx* muscle. No obvious signs of reduced SERCA transport efficiency can be seen in the D2 *mdx* muscles where both uptake and ATP hydrolysis were drastically reduced. Thus, these findings show that in 10–12-week-old C57 *mdx* mice, SLN does not dramatically cause impairments in SERCA function. Further, since less SLN was found in the D2 *mdx* muscles, it cannot explain the severe impairments in SERCA function. These findings are consistent with another study showing that SLN levels can vary between mouse strains [123], but also suggests that SLN may not always follow disease severity.

To determine the cellular basis behind the impairments in Ca^{2+} regulation in the D2 *mdx* mouse, additional western blotting was done. Both C57 and D2 *mdx* mice had an

increase in both SERCA isoforms, which may represent a compensatory response to bring Ca^{2+} into the SR during states of high Ca^{2+} stress. However, a clear upregulation in SERCA2a isoform was present in solely the D2 *mdx* mice, which has been shown in the quadriceps of the highly affected mdx/utrophin KO mice [84]. Further, the greater increases in SERCA2a, the slow fibre type SERCA isoform, may be more indicative of a fast-to-slow twitch muscle fibre compensatory change towards the DMD protective slow phenotype. Additionally, RyR1 content was reduced in both C57 and D2 *mdx* mice compared to their respective WTs. D2 WT also has a trending reduction in RyR1 content compared to C57 WT. The reduction in RyR1 content in the *mdx* mice is again reflective of a shift towards a slow fibre type. Interestingly, when calstabin - an important regulator of RyR channel leak is expressed as a ratio to RyR1, the calstabin: RyR1 ratio is much higher in the D2 *mdx* gastrocnemius. This indicates that there is likely much more calstabin binding to RyR1, which would inhibit the ability to leak Ca^{2+} from the SR, which correlates to the leak data in both leak assays. This may also be a compensatory relationship to reduce SR Ca^{2+} leak in a state of Ca^{2+} dysregulation.

Thus far, neither SLN, SERCA isoform or RyR examination can explain the dramatic reductions in SERCA function observed in the D2 *mdx* muscles. Quantification of total protein adducted nitrocysteine and nitrotyrosine found a much higher amount of RONS attached to proteins in the D2 *mdx* gastrocnemius. This suggests that only the D2 *mdx* mice have signs of elevated oxidative/nitrosative stress. Indeed, these RONS are known to modify proteins, including SERCA and RyR. For example, if RONS modifications change and subsequently impair SERCA's ATP and Ca^{2+} binding domains, this can lead to muscle damage and weakness [124,125]. When my blots were performed for total protein nitration in gastrocnemius, RONS were most prominent at approximately 110 kDa, the molecular weight of SERCA. Thus, it is highly likely that RONS may be inducing post-

translational modifications on the SERCA pumps in D2 *mdx* mice. Of even more interest, these blots were performed in standard SDS-PAGE (i.e., reducing) conditions, which would mean that it is likely that any present nitrocysteine or nitrotyrosine represents irreversible protein damage. In fact, when D2 *mdx* gastrocnemius were treated with DTT (a potent reducing agent) during the 96-well plate uptake and leak assay, they did not exhibit any improvements in SR Ca^{2+} handling. The presence of high cysteine and tyrosine nitration in reducing conditions, coupled with DTT treatment in the D2 *mdx* mice, indicate irreversible RONS modifications and SR Ca^{2+} handling damage in the gastrocnemius as early as 10 weeks of age. This is likely a major contributor to the impairments in SR Ca^{2+} handling in the D2 *mdx* mouse.

When Ca^{2+} is highly dysregulated in DMD, pathological outcomes perpetuate the disease, including increased calpain activation [126]. This study is the first to demonstrate that rates of calpain activity are higher in the D2 background compared to C57, irrespective of the *mdx* genotype. Furthermore, planned comparisons between D2 *mdx* and C57 *mdx* reveals a significant 2.2-fold increase in calpain activity in the former vs the latter (p = 0.0006 via Student's t-test). This finding is important and adds mechanistic insight that may partly explain the worsened pathology in the D2 *mdx* mouse. It is interesting that the D2 WT mice already had elevated calpain activation compared with C57 WT, and though I do not have an exact explanation, this apparent difference in background strain can also partially explain why the *mdx* mice on the DBA/2J background are worse off than *mdx* mice on the C57BL/10 background. One explanation that is not yet well understood, is a potential crosstalk between calpain activation and the pro-fibrotic factor TGF-β. A few works found that TGF-β1 upregulation in lung fibroblasts and atrial derived myocytes can increase calpain activation [127,128]. It is additionally understood that a polymorphism of

LTBP4 in D2 WT greatly upregulates TGF-β [129], suggesting that the increased TGF-β activity could increase calpain activity in the D2 WT mice. This combined with the impairments observed in SERCA function could contribute to elevated calpain in the D2 *mdx* mice.

Additionally, high intracellular Ca^{2+} can lead to mitochondrial dysfunction in DMD pathology. Elevated myoplasmic Ca^{2+} can increase intake of Ca^{2+} into the mitochondria which eventually leads to the opening of the mitochondrial permeability transition pore (mPTP), then swelling and bursting of the mitochondria, excessive H_2O_2 emission into the myoplasm, and subsequent calpain activation [130]. A recent study by Hughes and colleagues indeed found that D2 *mdx* mice have a greater number of swollen mitochondria, increased susceptibility to mPTP opening in the quadriceps and excessive H_2O_2 emission [131]. This could be contributing to the increased RONS released into the muscle and subsequent SR Ca^{2+} handling dysfunction.

In addition to calpain activation, SR Ca^{2+} dysregulation in the D2 *mdx* muscles may be a contributing factor to the elevated daily energy expenditure seen in the metabolic caging data. Considering the large reductions in cage ambulation, a high demand on Ca^{2+} regulation may contribute to the heightened energy expenditure in the D2 *mdx* mice. It is presumed that SERCA would be consuming a large amount of energy to try and limit myoplasmic Ca^{2+} levels in the D2 *mdx* muscles. SLN is a known mediator of muscle-based thermogenesis, and its overexpression has been linked to elevated daily energy expenditure, however, SLN was more elevated in C57 *mdx* muscles and only the D2 *mdx* mice had elevated daily energy expenditure. This high energetic demand could be due to the increased muscle wasting in the D2 *mdx* mice. Calpain is known to activate both apoptotic and necrotic events [132]. Apoptosis is known to be an active programmed process requiring energy, while the necrotic pathways are debated as active or passive

processes [133,134]. The ubiquitin-proteasome system acts to selectively degrade intracellular proteins and requires energy use through ATP hydrolysis [135]. The proteasome system and calpain system are also known to interact where increased calpain activity can increase proteasome-dependent proteolysis [136], which could add to energy expenditure in the D2 *mdx* mice.

In contrast to our energy expenditure results, a previous study in ~ 5-month-old C57 *mdx* and WT mice, where Strakova et al., (2018) found that although there are no significant differences in cage activity between C57 *mdx* and WT mice, the *mdx* phenotype results in significantly greater energy expenditure (normalized to bodyweight). These differences may be due to age differences between Strakova's study and ours. Another study found that at 8 weeks of age, *mdx*/utrophin double knock out mice have lower activity levels relative to oxygen consumption [137], which supports that some metabolic differences can occur at younger ages in more severe *mdx* models. Additionally, C57 *mdx* mice at 5 months of age are less able to maintain core temperature [138,139] which may contribute to an increase in non-shivering thermogenesis via futile Ca^{2+} cycling to maintain body temperature [140]. The hypermetabolic phenotype in slightly older C57 *mdx* mice likely occurs from this response to maintain body temperature in the cold. It would be of interest to determine whether D2 *mdx* mice are unable to maintain core temperature at the age used in this present study.

Strengths and Limitations

A strength of the study design is the comparison of both *mdx* models against their strain WT. This accounts for potential, and in our case, actual differences in strain that decrease the ability to directly compare the *mdx* models. Additionally, the age of the mice we used was a strength to determine the severity of Ca^{2+} dysfunction at a young age,

which would be a more reflective age of boys affected with DMD. As we can validate and replicate our uptake measures on a separate set of samples with the use of two different pieces of equipment strengthens our findings and highlights reproducibility. We were also able to determine that increased Ca^{2+} dysfunction was leading to pathologic Ca^{2+} pathways by determining calpain activation in our samples, and potentially alterations in energy expenditure.

Our study design did encounter limitations, which will be addressed in this section. A large change that had to be made during the study's course was the skeletal muscle tissue that was collected. Originally, we intended to collect the EDL to conduct these experiments, as it is a well-studied muscle in *mdx* experiments and demonstrates decrements in function in previous D2 *mdx* studies [102,105]. However, we had to switch our focus to the gastrocnemius muscle as our original uptake and leak assay required a large amount of tissue, and the EDLs of D2 *mdx* mice did not provide enough sample. However, the gastrocnemius proved to be an excellent substitute – it had great responsiveness in our assays, but more importantly, is a highly affected skeletal muscle in DMD [141,142], and had already been shown to be highly affected in the D2 *mdx* mouse [105,131]. Nevertheless, other muscles such as the diaphragm and cardiac muscle should be analyzed, especially considering the fact that most patients with DMD succumb to cardiorespiratory failure.

While our total protein analyses indicate elevated oxidative/nitrosative stress in the D2 *mdx* muscles, co-immunoprecipitation experiments with SERCA and RyR to determine direct protein RONS modifications would strengthen our conclusions. Furthermore, other SERCA regulators such as phospholamban and neuronatin – a novel SERCA regulator we have identified in skeletal muscle (Braun et al., 2021 [under review]) could provide further insight on SR Ca^{2+} handling in the D2 *mdx* mice. Although there is significant

evidence of the involvement of SERCA, RyR and RONS modifications in Ca^{2+}-related pathology in the *mdx* mouse, it is possible that other SR proteins or sarcolemmal channels may be influencing Ca^{2+} dysregulation. This could include DHPR, calsequestrin and store operated Ca^{2+} entry channels [143–145]. This is not an extensive list, nevertheless these factors among others should be considered in further Ca^{2+} handling characterization of the D2 *mdx* mouse.

Future Directions

This is the first study demonstrating that Ca^{2+} regulation, specifically at the level of the SERCA pump, is worsened in D2 *mdx* mice – the more phenotypical murine model of DMD. This knowledge leads into a critical question: will the improvement of SERCA function improve D2 *mdx* pathology? Previous work in other *mdx* models suggest that this could be true as displayed in the C57 *mdx* model. The overexpression of SERCA has demonstrated alleviation of DMD pathology in *mdx* and Sgcb-/- mice [85,87]. Relatable to our current study's findings, HSP72 can protect SERCA from oxidative stress. Pharmacological and genetic induction of HSP72 has been shown to mitigate dystrophic pathology in the C57 *mdx* and the *mdx*:utr knockout mice [88]. However, the improvement of SERCA function in previous studies have not always led to the improvement of *mdx* pathology. When Fajardo and colleagues genetically deleted SLN in the C57 *mdx* mice, SERCA function was slightly improved, but dystrophic pathology was actually worsened [95].This was due to an impairment in calcineurin activation, since SLN is also a well-known activator of calcineurin. Thus, in the absence of SLN, *mdx* mice had less utrophin and a smaller proportion of oxidative fibres. This is in contrast with other studies who have showed that SLN deletion improved maximal SERCA activity and uptake and mitigated dystrophic pathology [93], and another study that showed that SLN deletion had no effect

in *mdx* mice [146]. Though the reasons for this are unclear, it is speculated that SLN-inhibition of SERCA may operate in hormesis, and in the context of DMD, some inhibition of SERCA via SLN would be beneficial as it would stimulate calcineurin signalling. Furthermore, SLN would also be able to protect the SERCA pumps from oxidative/nitrosative stress, by physically binding to the SERCA and preventing oxidant damage [147]. However, too much SLN can lead to drastic impairments in SERCA function, perpetuating calcium dysregulation and dystrophic pathology. Considering the results from this thesis, it appears that SLN does not contribute to the worsened Ca^{2+} handling or disease severity in the D2 *mdx* muscles, since SLN was more upregulated in the C57 *mdx* muscles. Thus, future studies improving SERCA function in D2 *mdx* mice may need to look at alternative methods, outside of SLN alterations, to determine whether improving SERCA function can alleviate the disease.

A potential target of interest for intervention is the enzyme glycogen synthase kinase 3 (GSK3). Our lab group and others have demonstrated that GSK3 is a regulator of SERCA function as it can increase SERCA2 and HSP72 content [148,149]. A pharmacological inhibitor of GSK3, called tideglusib, is currently being tested in our lab with promising results of improved muscle function and reduced serum creatine kinase release. Tideglusib exerts its effect by irreversibly inhibiting GSK3, and is already in clinical trials for another distinct form of muscular dystrophy – called myotonic dystrophy type 1 [150–152]. Future studies should examine its effect on SR Ca^{2+} handling in cardiac and skeletal muscle. Aside from tideglusib or other GSK3 binding drugs could be explored, including lithium, a long-standing therapeutic used clinically which has also shown promise in SERCA content upregulation [149]. Finally, to fully determine the therapeutics role of GSK3 inhibition, muscle specific GSK3 deletion in the D2 *mdx* mouse could be explored.

Another study of importance would be a time-course study determining SR Ca^{2+} handling dysfunction in the D2 *mdx* mice through age. This would be important to conduct at earlier ages, up until the time-point of this study (10 weeks of age) to determine an ideal age of potential intervention in the D2 *mdx* mice before irreversible damage to muscle occurs. As other studies show distinct muscle damage in the D2 *mdx* mice by 8 weeks of age [102], early treatment is of great importance. The median age of DMD diagnosis in humans is approximately 5 years of age [153], which can be related to roughly 3-4 weeks of age in mice [154], making this an ideal age of intervention.

In conclusion, this study contributes novel knowledge of the SR Ca^{2+} handling phenotype in D2 *mdx* mice and future studies aimed at improving Ca^{2+} regulation in these mice may better inform on potential therapeutic strategies for patients living with DMD.

Chapter 6: Appendix

Appendix A

This AUP has been amended to include D2 *mdx* experiments.

Brock

Animal Care Committee (ACC)
Chair – Jim Willwerth, PhD 905.688.5550 ext 5477
Clinical Veterinarians – Dr. Alistair Ker
Animal Care Committee Coordinator – Dayle Carlson ext 5820

Date: June 22, 2017

Dear Dr. Fajardo and Dr. Roy,

The Animal Care Committee has approved your "Animal Use Protocol (AUP)" entitled:

Examining the effects of GSK3 inhibition skeletal muscle physiology and disease in mice.

This approval expires in one year on the last day of the month.
The number for this project is **AUP # 17 – 06 – 03**.
This number must be indicated when ordering animals for this project.

ANIMALS APPROVED:

Mouse	C57BL	Wild type	60 M
Mouse	C57BL/10	*Mdx*	20 M

REQUIREMENTS/COMMENTS
Please ensure that individual(s) performing procedures, as described in this protocol, are familiar with the contents of this document.

Jim Willwerth, Chair of ACC

THIS PROTOCOL IS IN EFFECT FOR A PERIOD OF ONE YEAR ONLY AND IS SUBJECT TO POST APPROVAL MONITORING.

ALL UNEXPECTED MORTALITIES MUST BE REPORTED TO ANIMAL CARE SERVICES STAFF IMMEDIATELY.

Appendix B

Co-immunoprecipitation (Co-IP) was conducted to examine SERCA1a/SERCA2a and RyR1 nitrosylation and nitration in gastrocnemius muscle. Calstabin binding to RyR1 was also measured. RyR1 and SERCA (1a and 2a) antibodies (5 μg) were conjugated to protein G magnetic beads (50 μg) (Surebeads #161-4023, BioRad). The antibody-protein G complex was then incubated with muscle homogenate (75 μg) for an hour at room temperature. SERCA1a/SERCA2a and RyR1 proteins and interacting proteins were then eluted using non-reducing (nitrosylation and nitration) 1x Laemmli buffer at 70°C for 10 minutes. western blotting (as described above) was then used to quantify levels of nitrosylation and nitration in the eluent of SERCA1a/SERCA2a and RyR1. All nitrosylation, nitration and calstabin levels were then normalized to the amount of respective protein of interest in the eluent after western blotting.

Table 3.2: Western Blotting Conditions for Co-IP Experiments

	Membrane	Running Conditi-ons	Transfer Conditi-ons	Membrane	Primary Dilution	Secondary Type & Dilution	Chemilum ine-scent Substrate
SERCA1 a/2a	TGX Precast	22 min at 240V	6 min turbo	PVDF	1:20,000	Anti-mouse; 1:20,000	Immobilon
RyR1	TGX Precast	45 min at 240V	6 min turbo	PVDF	1:1,000	Anti-mouse	Immobilon
Calstabi n1	TGX Precast	22 min at 240V	6 min turbo	PVDF	1:5,000	Anti-rabbit	Femto West
Tyrosine: SERCA	TGX Precast	22 min at 240V	6 min turbo	PVDF	1:2,000	Anti-mouse	Immobilon
Cysteine: SERCA	TGX Precast	22 min at 240V	6 min turbo	PVDF	1:2,000	Anti-mouse	Immobilon

Appendix C

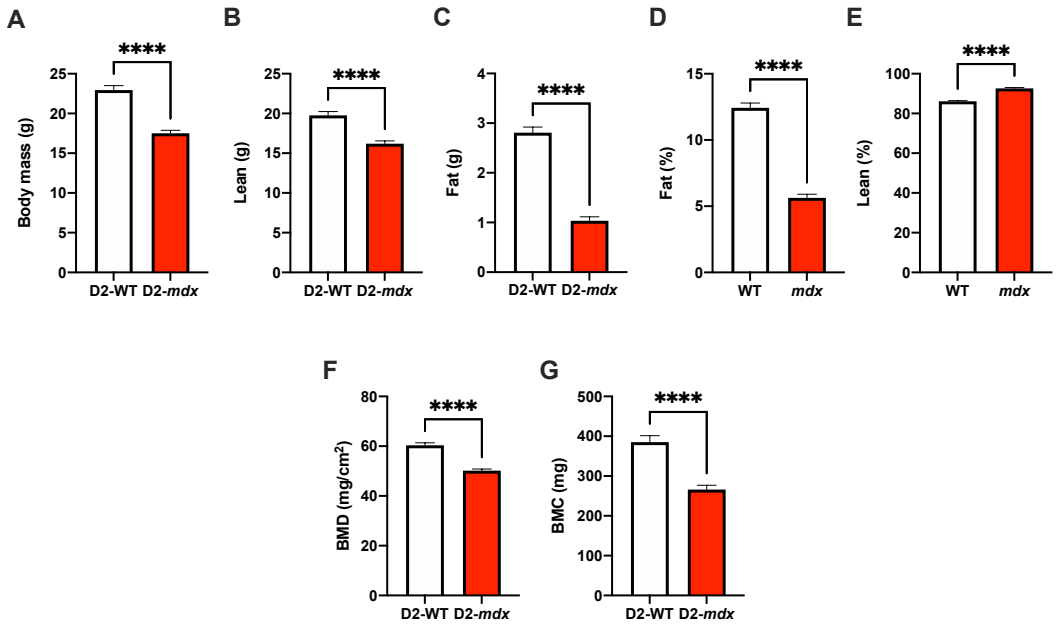

Figure 1 (Appendix C): Body Compositions of D2 WT and D2 *mdx* mice. A) demonstrates differences in body mass in grams. B) Lean mass in grams. C) Fat mass in grams. D) Percent of fat mass. E) Percent of lean mass. F) Bone mineral density (mg/cm^2). G) Bone mineral content (mg). A Students' t-test was used for all comparisons.

References

1. Moat, S.J.; Bradley, D.M.; Salmon, R.; Clarke, A.; Hartley, L. Newborn Bloodspot Screening for Duchenne Muscular Dystrophy: 21 Years Experience in Wales (UK). *Eur. J. Hum. Genet. EJHG* **2013**, *21*, 1049–1053, doi:10.1038/ejhg.2012.301.
2. Emery, A.E. Population Frequencies of Inherited Neuromuscular Diseases--a World Survey. *Neuromuscul. Disord. NMD* **1991**, *1*, 19–29, doi:10.1016/0960-8966(91)90039-u.
3. Straub, V.; Balabanov, P.; Bushby, K.; Ensini, M.; Goemans, N.; De Luca, A.; Pereda, A.; Hemmings, R.; Campion, G.; Kaye, E.; et al. Stakeholder Cooperation to Overcome Challenges in Orphan Medicine Development: The Example of Duchenne Muscular Dystrophy. *Lancet Neurol.* **2016**, *15*, 882–890, doi:10.1016/S1474-4422(16)30035-7.
4. Emery, A.E.H. The Muscular Dystrophies. *Lancet Lond. Engl.* **2002**, *359*, 687–695, doi:10.1016/S0140-6736(02)07815-7.
5. *Duchenne Muscular Dystrophy*; Oxford Monographs on Medical Genetics; Fourth Edition.; Oxford University Press: Oxford, New York, 2015; ISBN 978-0-19-968148-8.
6. Grigore, I.; Frasin, M.; Diaconu, G. CARDIAC COMPLICATIONS IN DUCHENNE MUSCULAR DYSTROPHY IN CHILDREN. *Romanian Journal of Pediatrics* **2015**, *64*, 5, doi:10.37897/RJP.2015.4.4.
7. Bladen, C.L.; Salgado, D.; Monges, S.; Foncuberta, M.E.; Kekou, K.; Kosma, K.; Dawkins, H.; Lamont, L.; Roy, A.J.; Chamova, T.; et al. The TREAT-NMD DMD Global Database: Analysis of More than 7,000 Duchenne Muscular Dystrophy Mutations. *Hum. Mutat.* **2015**, *36*, 395–402, doi:10.1002/humu.22758.
8. Hoffman, E.P.; Brown, R.H.; Kunkel, L.M. Dystrophin: The Protein Product of the Duchenne Muscular Dystrophy Locus. *Cell* **1987**, *51*, 919–928, doi:10.1016/0092-8674(87)90579-4.
9. Blake, D.J.; Weir, A.; Newey, S.E.; Davies, K.E. Function and Genetics of Dystrophin and Dystrophin-Related Proteins in Muscle. *Physiol. Rev.* **2002**, *82*, 291–329, doi:10.1152/physrev.00028.2001.
10. Dumont, N.A.; Bentzinger, C.F.; Sincennes, M.-C.; Rudnicki, M.A. Satellite Cells and Skeletal Muscle Regeneration. In *Comprehensive Physiology*; Terjung, R., Ed.; John Wiley & Sons, Inc.: Hoboken, NJ, USA, 2015; pp. 1027–1059 ISBN 978-0-470-65071-4.
11. Schmalbruch, H. Regenerated Muscle Fibers in Duchenne Muscular Dystrophy: A Serial Section Study. *Neurology* **1984**, *34*, 60–60, doi:10.1212/WNL.34.1.60.
12. McDouall, R.M.; Dunn, M.J.; Dubowitz, V. Nature of the Mononuclear Infiltrate and the Mechanism of Muscle Damage in Juvenile Dermatomyositis and Duchenne Muscular Dystrophy. *J. Neurol. Sci.* **1990**, *99*, 199–217, doi:10.1016/0022-510X(90)90156-H.
13. Bockhold, K.J.; Rosenblatt, J.D.; Partridge, T.A. Aging Normal and Dystrophic Mouse Muscle: Analysis of Myogenicity in Cultures of Living Single Fibers. *Muscle Nerve* **1998**, *21*, 173–183, doi:10.1002/(sici)1097-4598(199802)21:2<173::aid-mus4>3.0.co;2-8.
14. Tubridy, N.; Fontaine, B.; Eymard, B. Congenital Myopathies and Congenital Muscular Dystrophies. *Curr. Opin. Neurol.* **2001**, *14*, 575–582, doi:10.1097/00019052-200110000-00005.

15. Shin, J.; Tajrishi, M.M.; Ogura, Y.; Kumar, A. Wasting Mechanisms in Muscular Dystrophy. *Int. J. Biochem. Cell Biol.* **2013**, *45*, 2266–2279, doi:10.1016/j.biocel.2013.05.001.
16. Endo, M. Calcium Ion as a Second Messenger With Special Reference to Excitation-Contraction Coupling. *J. Pharmacol. Sci.* **2006**, *100*, 519–524, doi:10.1254/jphs.CPJ06004X.
17. Jurkat-Rott, K.; Fauler, M.; Lehmann-Horn, F. Ion Channels and Ion Transporters of the Transverse Tubular System of Skeletal Muscle. *J. Muscle Res. Cell Motil.* **2006**, *27*, 275–290, doi:10.1007/s10974-006-9088-z.
18. Franzini-Armstrong, C.; Protasi, F.; Ramesh, V. Shape, Size, and Distribution of Ca2+ Release Units and Couplons in Skeletal and Cardiac Muscles. *Biophys. J.* **1999**, *77*, 1528–1539, doi:10.1016/S0006-3495(99)77000-1.
19. Santulli, G.; Lewis, D.; des Georges, A.; Marks, A.R.; Frank, J. Ryanodine Receptor Structure and Function in Health and Disease. *Subcell. Biochem.* **2018**, *87*, 329–352, doi:10.1007/978-981-10-7757-9_11.
20. Schiaffino, S.; Reggiani, C. Fiber Types in Mammalian Skeletal Muscles. *Physiol. Rev.* **2011**, *91*, 1447–1531, doi:10.1152/physrev.00031.2010.
21. MacLennan, D.H.; Rice, W.J.; Green, N.M. The Mechanism of Ca $^{2+}$ Transport by Sarco(Endo)Plasmic Reticulum Ca $^{2+}$ -ATPases. *J. Biol. Chem.* **1997**, *272*, 28815–28818, doi:10.1074/jbc.272.46.28815.
22. Berchtold, M.W.; Brinkmeier, H.; Müntener, M. Calcium Ion in Skeletal Muscle: Its Crucial Role for Muscle Function, Plasticity, and Disease. *Physiol. Rev.* **2000**, *80*, 1215–1265, doi:10.1152/physrev.2000.80.3.1215.
23. Turner, P.R.; Westwood, T.; Regen, C.M.; Steinhardt, R.A. Increased Protein Degradation Results from Elevated Free Calcium Levels Found in Muscle from Mdx Mice. *Nature* **1988**, *335*, 735–738, doi:10.1038/335735a0.
24. Robert, V.; Massimino, M.L.; Tosello, V.; Marsault, R.; Cantini, M.; Sorrentino, V.; Pozzan, T. Alteration in Calcium Handling at the Subcellular Level in Mdx Myotubes. *J. Biol. Chem.* **2001**, *276*, 4647–4651, doi:10.1074/jbc.M006337200.
25. Spencer, M.J. Overexpression of a Calpastatin Transgene in Mdx Muscle Reduces Dystrophic Pathology. *Hum. Mol. Genet.* **2002**, *11*, 2645–2655, doi:10.1093/hmg/11.21.2645.
26. Chapa-Dubocq, X.; Makarov, V.; Javadov, S. Simple Kinetic Model of Mitochondrial Swelling in Cardiac Cells. *J. Cell. Physiol.* **2018**, *233*, 5310–5321, doi:10.1002/jcp.26335.
27. Efremov, R.G.; Leitner, A.; Aebersold, R.; Raunser, S. Architecture and Conformational Switch Mechanism of the Ryanodine Receptor. *Nature* **2015**, *517*, 39–43, doi:10.1038/nature13916.
28. Takeshima, H.; Nishimura, S.; Matsumoto, T.; Ishida, H.; Kangawa, K.; Minamino, N.; Matsuo, H.; Ueda, M.; Hanaoka, M.; Hirose, T.; et al. Primary Structure and Expression from Complementary DNA of Skeletal Muscle Ryanodine Receptor. *Nature* **1989**, *339*, 439–445, doi:10.1038/339439a0.
29. Nakai, J.; Imagawa, T.; Hakamat, Y.; Shigekawa, M.; Takeshima, H.; Numa, S. Primary Structure and Functional Expression from CDNA of the Cardiac Ryanodine Receptor/Calcium Release Channel. *FEBS Lett.* **1990**, *271*, 169–177, doi:10.1016/0014-5793(90)80399-4.
30. Otsu, K.; Willard, H.F.; Khanna, V.K.; Zorzato, F.; Green, N.M.; MacLennan, D.H. Molecular Cloning of CDNA Encoding the Ca2+ Release Channel (Ryanodine

Receptor) of Rabbit Cardiac Muscle Sarcoplasmic Reticulum. *J. Biol. Chem.* **1990**, *265*, 13472–13483.
31. Brillantes, A.M.; Allen, P.; Takahashi, T.; Izumo, S.; Marks, A.R. Differences in Cardiac Calcium Release Channel (Ryanodine Receptor) Expression in Myocardium from Patients with End-Stage Heart Failure Caused by Ischemic versus Dilated Cardiomyopathy. *Circ. Res.* **1992**, *71*, 18–26, doi:10.1161/01.res.71.1.18.
32. Nakashima, Y.; Nishimura, S.; Maeda, A.; Barsoumian, E.L.; Hakamata, Y.; Nakai, J.; Allen, P.D.; Imoto, K.; Kita, T. Molecular Cloning and Characterization of a Human Brain Ryanodine Receptor [1]. *FEBS Lett.* **1997**, *417*, 157–162, doi:10.1016/S0014-5793(97)01275-1.
33. Hakamata, Y.; Nakai, J.; Takeshima, H.; Imoto, K. Primary Structure and Distribution of a Novel Ryanodine Receptor/Calcium Release Channel from Rabbit Brain. *FEBS Lett.* **1992**, *312*, 229–235, doi:10.1016/0014-5793(92)80941-9.
34. Zhang, L.; Liu, Y.; Song, F.; Zheng, H.; Hu, L.; Lu, H.; Liu, P.; Hao, X.; Zhang, W.; Chen, K. Functional SNP in the MicroRNA-367 Binding Site in the 3'UTR of the Calcium Channel Ryanodine Receptor Gene 3 (RYR3) Affects Breast Cancer Risk and Calcification. *Proc. Natl. Acad. Sci.* **2011**, *108*, 13653–13658, doi:10.1073/pnas.1103360108.
35. Lanner, J.T.; Georgiou, D.K.; Joshi, A.D.; Hamilton, S.L. Ryanodine Receptors: Structure, Expression, Molecular Details, and Function in Calcium Release. *Cold Spring Harb. Perspect. Biol.* **2010**, *2*, a003996–a003996, doi:10.1101/cshperspect.a003996.
36. Uhlen, M.; Fagerberg, L.; Hallstrom, B.M.; Lindskog, C.; Oksvold, P.; Mardinoglu, A.; Sivertsson, A.; Kampf, C.; Sjostedt, E.; Asplund, A.; et al. Tissue-Based Map of the Human Proteome. *Science* **2015**, *347*, 1260419–1260419, doi:10.1126/science.1260419.
37. Inui, M.; Saito, A.; Fleischer, S. Purification of the Ryanodine Receptor and Identity with Feet Structures of Junctional Terminal Cisternae of Sarcoplasmic Reticulum from Fast Skeletal Muscle. *J. Biol. Chem.* **1987**, *262*, 1740–1747.
38. Marks, A.R.; Tempst, P.; Hwang, K.S.; Taubman, M.B.; Inui, M.; Chadwick, C.; Fleischer, S.; Nadal-Ginard, B. Molecular Cloning and Characterization of the Ryanodine Receptor/Junctional Channel Complex CDNA from Skeletal Muscle Sarcoplasmic Reticulum. *Proc. Natl. Acad. Sci. U. S. A.* **1989**, *86*, 8683–8687, doi:10.1073/pnas.86.22.8683.
39. Bannister, R.A. Bridging the Myoplasmic Gap II: More Recent Advances in Skeletal Muscle Excitation–Contraction Coupling. *J. Exp. Biol.* **2016**, *219*, 175–182, doi:10.1242/jeb.124123.
40. Bloemberg, D.; Quadrilatero, J. Rapid Determination of Myosin Heavy Chain Expression in Rat, Mouse, and Human Skeletal Muscle Using Multicolor Immunofluorescence Analysis. *PLoS ONE* **2012**, *7*, e35273, doi:10.1371/journal.pone.0035273.
41. Bastide, B.; Mounier, Y. Single-Channel Properties of the Sarcoplasmic Reticulum Calcium-Release Channel in Slow- and Fast-Twitch Muscles of Rhesus Monkeys. *Pfl□gers Arch. Eur. J. Physiol.* **1998**, *436*, 485–488, doi:10.1007/s004240050661.
42. Delbono, O.; Meissner, G. Sarcoplasmic Reticulum Ca 2+ Release in Rat Slow- and Fast-Twitch Muscles. *J. Membr. Biol.* **1996**, *151*, 123–130, doi:10.1007/s002329900063.

43. Calderón, J.C. Enzymatic Dissociation of Long Muscles from Mice: A Model for the Study of Skeletal Muscle Fiber Types. **2013**, *26*, 10.
44. Bezprozvanny, Ilya; Watras, J.; Ehrlich, B.E. Bell-Shaped Calcium-Response Curves of Lns(l,4,5)P3- and Calcium-Gated Channels from Endoplasmic Reticulum of Cerebellum. *Nature* **1991**, *351*, 751–754, doi:10.1038/351751a0.
45. Smith, J.S.; Coronado, R.; Meissner, G. Single Channel Measurements of the Calcium Release Channel from Skeletal Muscle Sarcoplasmic Reticulum. Activation by Ca2+ and ATP and Modulation by Mg2+. *J. Gen. Physiol.* **1986**, *88*, 573–588, doi:10.1085/jgp.88.5.573.
46. Laver, D.R. Regulation of the RyR Channel Gating by Ca2+ and Mg2+. *Biophys. Rev.* **2018**, *10*, 1087–1095, doi:10.1007/s12551-018-0433-4.
47. des Georges, A.; Clarke, O.B.; Zalk, R.; Yuan, Q.; Condon, K.J.; Grassucci, R.A.; Hendrickson, W.A.; Marks, A.R.; Frank, J. Structural Basis for Gating and Activation of RyR1. *Cell* **2016**, *167*, 145-157.e17, doi:10.1016/j.cell.2016.08.075.
48. Porta, M.; Zima, A.V.; Nani, A.; Diaz-Sylvester, P.L.; Copello, J.A.; Ramos-Franco, J.; Blatter, L.A.; Fill, M. Single Ryanodine Receptor Channel Basis of Caffeine's Action on Ca2+ Sparks. *Biophys. J.* **2011**, *100*, 931–938, doi:10.1016/j.bpj.2011.01.017.
49. Zalk, R.; Clarke, O.B.; des Georges, A.; Grassucci, R.A.; Reiken, S.; Mancia, F.; Hendrickson, W.A.; Frank, J.; Marks, A.R. Structure of a Mammalian Ryanodine Receptor. *Nature* **2015**, *517*, 44–49, doi:10.1038/nature13950.
50. Breckner, A.; Ganz, M.; Marcellin, D.; Richter, J.; Gerwin, N.; Rausch, M. Effect of Calstabin1 Depletion on Calcium Transients and Energy Utilization in Muscle Fibers and Treatment Opportunities with RyR1 Stabilizers. *PLoS ONE* **2013**, *8*, e81277, doi:10.1371/journal.pone.0081277.
51. Gaburjakova, M.; Gaburjakova, J.; Reiken, S.; Huang, F.; Marx, S.O.; Rosemblit, N.; Marks, A.R. FKBP12 Binding Modulates Ryanodine Receptor Channel Gating. *J. Biol. Chem.* **2001**, *276*, 16931–16935, doi:10.1074/jbc.M100856200.
52. Rhoads, A.R.; Friedberg, F. Sequence Motifs for Calmodulin Recognition. *FASEB J.* **1997**, *11*, 331–340, doi:10.1096/fasebj.11.5.9141499.
53. Rodney, G.G.; Moore, C.P.; Williams, B.Y.; Zhang, J.Z.; Krol, J.; Pedersen, S.E.; Hamilton, S.L. Calcium Binding to Calmodulin Leads to an N-Terminal Shift in Its Binding Site on the Ryanodine Receptor. *J. Biol. Chem.* **2001**, *276*, 2069–2074, doi:10.1074/jbc.M008891200.
54. Boschek, C.B.; Jones, T.E.; Smallwood, H.S.; Squier, T.C.; Bigelow, D.J. Loss of the Calmodulin-Dependent Inhibition of the RyR1 Calcium Release Channel upon Oxidation of Methionines in Calmodulin †. *Biochemistry* **2008**, *47*, 131–142, doi:10.1021/bi701352w.
55. Witherspoon, J.W.; Meilleur, K.G. Review of RyR1 Pathway and Associated Pathomechanisms. *Acta Neuropathol. Commun.* **2016**, *4*, 121, doi:10.1186/s40478-016-0392-6.
56. Reiken, S.; Lacampagne, A.; Zhou, H.; Kherani, A.; Lehnart, S.E.; Ward, C.; Huang, F.; Gaburjakova, M.; Gaburjakova, J.; Rosemblit, N.; et al. PKA Phosphorylation Activates the Calcium Release Channel (Ryanodine Receptor) in Skeletal Muscle. *J. Cell Biol.* **2003**, *160*, 919–928, doi:10.1083/jcb.200211012.
57. Bellinger, A.M.; Reiken, S.; Dura, M.; Murphy, P.W.; Deng, S.-X.; Landry, D.W.; Nieman, D.; Lehnart, S.E.; Samaru, M.; LaCampagne, A.; et al. Remodeling of Ryanodine Receptor Complex Causes "Leaky" Channels: A Molecular Mechanism

for Decreased Exercise Capacity. *Proc. Natl. Acad. Sci.* **2008**, *105*, 2198–2202, doi:10.1073/pnas.0711074105.
58. Aracena-Parks, P.; Goonasekera, S.A.; Gilman, C.P.; Dirksen, R.T.; Hidalgo, C.; Hamilton, S.L. Identification of Cysteines Involved in *S* -Nitrosylation, *S* -Glutathionylation, and Oxidation to Disulfides in Ryanodine Receptor Type 1. *J. Biol. Chem.* **2006**, *281*, 40354–40368, doi:10.1074/jbc.M600876200.
59. Barreiro, E.; Hussain, S.N.A. Protein Carbonylation in Skeletal Muscles: Impact on Function. *Antioxid. Redox Signal.* **2010**, *12*, 417–429, doi:10.1089/ars.2009.2808.
60. Aracena, P.; Sánchez, G.; Donoso, P.; Hamilton, S.L.; Hidalgo, C. *S* -Glutathionylation Decreases Mg^{2+} Inhibition and *S* -Nitrosylation Enhances Ca^{2+} Activation of RyR1 Channels. *J. Biol. Chem.* **2003**, *278*, 42927–42935, doi:10.1074/jbc.M306969200.
61. Sun, J.; Xin, C.; Eu, J.P.; Stamler, J.S.; Meissner, G. Cysteine-3635 Is Responsible for Skeletal Muscle Ryanodine Receptor Modulation by NO. *Proc. Natl. Acad. Sci.* **2001**, *98*, 11158–11162, doi:10.1073/pnas.201289098.
62. Ferdinandy, P. Peroxynitrite: Just an Oxidative/Nitrosative Stressor or a Physiological Regulator as Well?: Commentary. *Br. J. Pharmacol.* **2009**, *148*, 1–3, doi:10.1038/sj.bjp.0706693.
63. Aracena, P.; Tang, W.; Hamilton, S.L.; Hidalgo, C. Effects of *S* -Glutathionylation and *S* -Nitrosylation on Calmodulin Binding to Triads and FKBP12 Binding to Type 1 Calcium Release Channels. *Antioxid. Redox Signal.* **2005**, *7*, 870–881, doi:10.1089/ars.2005.7.870.
64. Andersson, D.C.; Meli, A.C.; Reiken, S.; Betzenhauser, M.J.; Umanskaya, A.; Shiomi, T.; D'Armiento, J.; Marks, A.R. Leaky Ryanodine Receptors in β-Sarcoglycan Deficient Mice: A Potential Common Defect in Muscular Dystrophy. *Skelet. Muscle* **2012**, *2*, 9, doi:10.1186/2044-5040-2-9.
65. Bellinger, A.M.; Reiken, S.; Carlson, C.; Mongillo, M.; Liu, X.; Rothman, L.; Matecki, S.; Lacampagne, A.; Marks, A.R. Hypernitrosylated Ryanodine Receptor/Calcium Release Channels Are Leaky in Dystrophic Muscle. *Nat. Med.* **2009**, *15*, 325–330, doi:10.1038/nm.1916.
66. Periasamy, M.; Kalyanasundaram, A. SERCA Pump Isoforms: Their Role in Calcium Transport and Disease. *Muscle Nerve* **2007**, *35*, 430–442, doi:10.1002/mus.20745.
67. Toyoshima, C. How Ca2+-ATPase Pumps Ions across the Sarcoplasmic Reticulum Membrane. *Biochim. Biophys. Acta BBA - Mol. Cell Res.* **2009**, *1793*, 941–946, doi:10.1016/j.bbamcr.2008.10.008.
68. Toyoshima, C.; Nakasako, M.; Nomura, H.; Ogawa, H. Crystal Structure of the Calcium Pump of Sarcoplasmic Reticulum at 2.6 Å Resolution. *Nature* **2000**, *405*, 647–655, doi:10.1038/35015017.
69. Toyoshima, C. Structural Aspects of Ion Pumping by Ca2+-ATPase of Sarcoplasmic Reticulum. *Arch. Biochem. Biophys.* **2008**, *476*, 3–11, doi:10.1016/j.abb.2008.04.017.
70. Clarke, D.M.; Loo, T.W.; Inesi, G.; MacLennan, D.H. Location of High Affinity Ca2 +-Binding Sites within the Predicted Transmembrahe Domain of the Sarco-Plasmic Reticulum Ca2+-ATPase. *Nature* **1989**, *339*, 476–478, doi:10.1038/339476a0.
71. Wu, K.D.; Lytton, J. Molecular Cloning and Quantification of Sarcoplasmic Reticulum Ca(2+)-ATPase Isoforms in Rat Muscles. *Am. J. Physiol.-Cell Physiol.* **1993**, *264*, C333–C341, doi:10.1152/ajpcell.1993.264.2.C333.

72. Fajardo, V.A.; Bombardier, E.; Vigna, C.; Devji, T.; Bloemberg, D.; Gamu, D.; Gramolini, A.O.; Quadrilatero, J.; Tupling, A.R. Co-Expression of SERCA Isoforms, Phospholamban and Sarcolipin in Human Skeletal Muscle Fibers. *PLoS ONE* **2013**, *8*, e84304, doi:10.1371/journal.pone.0084304.
73. Smith, I.C.; Bombardier, E.; Vigna, C.; Tupling, A.R. ATP Consumption by Sarcoplasmic Reticulum Ca2+ Pumps Accounts for 40-50% of Resting Metabolic Rate in Mouse Fast and Slow Twitch Skeletal Muscle. *PLoS ONE* **2013**, *8*, e68924, doi:10.1371/journal.pone.0068924.
74. Asahi, M.; Kurzydlowski, K.; Tada, M.; MacLennan, D.H. Sarcolipin Inhibits Polymerization of Phospholamban to Induce Superinhibition of Sarco(Endo)Plasmic Reticulum Ca2+-ATPases (SERCAs). *J. Biol. Chem.* **2002**, *277*, 26725–26728, doi:10.1074/jbc.C200269200.
75. Wegener, A.D.; Simmerman, H.K.; Lindemann, J.P.; Jones, L.R. Phospholamban Phosphorylation in Intact Ventricles. Phosphorylation of Serine 16 and Threonine 17 in Response to Beta-Adrenergic Stimulation. *J. Biol. Chem.* **1989**, *264*, 11468–11474.
76. Simmerman, H.K.; Collins, J.H.; Theibert, J.L.; Wegener, A.D.; Jones, L.R. Sequence Analysis of Phospholamban. Identification of Phosphorylation Sites and Two Major Structural Domains. *J. Biol. Chem.* **1986**, *261*, 13333–13341.
77. MacLennan, D.H.; Kranias, E.G. Phospholamban: A Crucial Regulator of Cardiac Contractility. *Nat. Rev. Mol. Cell Biol.* **2003**, *4*, 566–577, doi:10.1038/nrm1151.
78. Odermatt, A.; Becker, S.; Khanna, V.K.; Kurzydlowski, K.; Leisner, E.; Pette, D.; MacLennan, D.H. Sarcolipin Regulates the Activity of SERCA1, the Fast-Twitch Skeletal Muscle Sarcoplasmic Reticulum Ca^{2+}-ATPase. *J. Biol. Chem.* **1998**, *273*, 12360–12369, doi:10.1074/jbc.273.20.12360.
79. Viner, R.I.; Williams, T.D.; Schöneich, C. Peroxynitrite Modification of Protein Thiols: Oxidation, Nitrosylation, and S-Glutathiolation of Functionally Important Cysteine Residue(s) in the Sarcoplasmic Reticulum Ca-ATPase †. *Biochemistry* **1999**, *38*, 12408–12415, doi:10.1021/bi9909445.
80. Viner, R.I.; Ferrington, D.A.; Hühmer, A.F.R.; Bigelow, D.J.; Schöneich, C. Accumulation of Nitrotyrosine on the SERCA2a Isoform of SR Ca-ATPase of Rat Skeletal Muscle during Aging: A Peroxynitrite-Mediated Process? *FEBS Lett.* **1996**, *379*, 286–290, doi:10.1016/0014-5793(95)01530-2.
81. Tupling, A.R.; Vigna, C.; Ford, R.J.; Tsuchiya, S.C.; Graham, D.A.; Denniss, S.G.; Rush, J.W.E. Effects of Buthionine Sulfoximine Treatment on Diaphragm Contractility and SR Ca^{2+} Pump Function in Rats. *J. Appl. Physiol.* **2007**, *103*, 1921–1928, doi:10.1152/japplphysiol.00529.2007.
82. Žižková, P.; Viskupičová, J.; Blaškovič, D.; Štrosová, M.K.; Žarkovič, N.; Horáková, Ľ. Sarcoplasmic Reticulum Ca^{2+}-ATPase from Rabbit Skeletal Muscle Modified by Peroxynitrite. *J. Enzyme Inhib. Med. Chem.* **2014**, *29*, 563–570, doi:10.3109/14756366.2013.827676.
83. Viner, R.I.; Hühmer, A.F.R.; Bigelow, D.J.; Schöneich, C. The Oxidative Inactivation of Sarcoplasmic Reticulum Ca^{2+}-ATPase by Peroxynitrite. *Free Radic. Res.* **1996**, *24*, 243–259, doi:10.3109/10715769609088022.
84. Schneider, J.S.; Shanmugam, M.; Gonzalez, J.P.; Lopez, H.; Gordan, R.; Fraidenraich, D.; Babu, G.J. Increased Sarcolipin Expression and Decreased Sarco(Endo)Plasmic Reticulum Ca2+ Uptake in Skeletal Muscles of Mouse Models of Duchenne Muscular Dystrophy. *J. Muscle Res. Cell Motil.* **2013**, *34*, 349–356, doi:10.1007/s10974-013-9350-0.

85. Goonasekera, S.A.; Lam, C.K.; Millay, D.P.; Sargent, M.A.; Hajjar, R.J.; Kranias, E.G.; Molkentin, J.D. Mitigation of Muscular Dystrophy in Mice by SERCA Overexpression in Skeletal Muscle. *J. Clin. Invest.* **2011**, *121*, 1044–1052, doi:10.1172/JCI43844.
86. Leberer, E.; Härtner, K.T.; Pette, D. Postnatal Development of Ca2+-Sequestration by the Sarcoplasmic Reticulum of Fast and Slow Muscles in Normal and Dystrophic Mice. *Eur. J. Biochem.* **1988**, *174*, 247–253, doi:10.1111/j.1432-1033.1988.tb14090.x.
87. Morine, K.J.; Sleeper, M.M.; Barton, E.R.; Sweeney, H.L. Overexpression of SERCA1a in the Mdx Diaphragm Reduces Susceptibility to Contraction-Induced Damage. *Hum. Gene Ther.* **2010**, *21*, 1735–1739, doi:10.1089/hum.2010.077.
88. Gehrig, S.M.; van der Poel, C.; Sayer, T.A.; Schertzer, J.D.; Henstridge, D.C.; Church, J.E.; Lamon, S.; Russell, A.P.; Davies, K.E.; Febbraio, M.A.; et al. Hsp72 Preserves Muscle Function and Slows Progression of Severe Muscular Dystrophy. *Nature* **2012**, *484*, 394–398, doi:10.1038/nature10980.
89. Hamstra, S.I.; Whitley, K.C.; Baranowski, R.W.; Kurgan, N.; Braun, J.L.; Messner, H.N.; Fajardo, V.A. The Role of Phospholamban and GSK3 in Regulating Rodent Cardiac SERCA Function. *Am. J. Physiol. Cell Physiol.* **2020**, doi:10.1152/ajpcell.00318.2020.
90. Fu, M.H.; Tupling, A.R. Protective Effects of Hsp70 on the Structure and Function of SERCA2a Expressed in HEK-293 Cells during Heat Stress. *Am. J. Physiol. Heart Circ. Physiol.* **2009**, *296*, H1175-1183, doi:10.1152/ajpheart.01276.2008.
91. Tupling, A.R.; Bombardier, E.; Vigna, C.; Quadrilatero, J.; Fu, M. Interaction between Hsp70 and the SR Ca2+ Pump: A Potential Mechanism for Cytoprotection in Heart and Skeletal Muscle. *Appl. Physiol. Nutr. Metab. Physiol. Appl. Nutr. Metab.* **2008**, *33*, 1023–1032, doi:10.1139/H08-067.
92. Fajardo, V.A.; Bombardier, E.; McMillan, E.; Tran, K.; Wadsworth, B.J.; Gamu, D.; Hopf, A.; Vigna, C.; Smith, I.C.; Bellissimo, C.; et al. Phospholamban Overexpression in Mice Causes a Centronuclear Myopathy-like Phenotype. *Dis. Model. Mech.* **2015**, *8*, 999–1009, doi:10.1242/dmm.020859.
93. Voit, A.; Patel, V.; Pachon, R.; Shah, V.; Bakhutma, M.; Kohlbrenner, E.; McArdle, J.J.; Dell'Italia, L.J.; Mendell, J.R.; Xie, L.-H.; et al. Reducing Sarcolipin Expression Mitigates Duchenne Muscular Dystrophy and Associated Cardiomyopathy in Mice. *Nat. Commun.* **2017**, *8*, doi:10.1038/s41467-017-01146-7.
94. Tanihata, J.; Nagata, T.; Ito, N.; Saito, T.; Nakamura, A.; Minamisawa, S.; Aoki, Y.; Ruegg, U.T.; Takeda, S. Truncated Dystrophin Ameliorates the Dystrophic Phenotype of Mdx Mice by Reducing Sarcolipin-Mediated SERCA Inhibition. *Biochem. Biophys. Res. Commun.* **2018**, *505*, 51–59, doi:10.1016/j.bbrc.2018.09.039.
95. Fajardo, V.A.; Chambers, P.J.; Juracic, E.S.; Rietze, B.A.; Gamu, D.; Bellissimo, C.; Kwon, F.; Quadrilatero, J.; Russell Tupling, A. Sarcolipin Deletion in Mdx Mice Impairs Calcineurin Signalling and Worsens Dystrophic Pathology. *Hum. Mol. Genet.* **2018**, *27*, 4094–4102, doi:10.1093/hmg/ddy302.
96. Bulfield, G.; Siller, W.G.; Wight, P.A.; Moore, K.J. X Chromosome-Linked Muscular Dystrophy (Mdx) in the Mouse. *Proc. Natl. Acad. Sci. U. S. A.* **1984**, *81*, 1189–1192.

97. Sicinski, P.; Geng, Y.; Ryder-Cook, A.S.; Barnard, E.A.; Darlison, M.G.; Barnard, P.J. The Molecular Basis of Muscular Dystrophy in the Mdx Mouse: A Point Mutation. *Science* **1989**, *244*, 1578–1580, doi:10.1126/science.2662404.
98. Ryder-Cook, A.S.; Sicinski, P.; Thomas, K.; Davies, K.E.; Worton, R.G.; Barnard, E.A.; Darlison, M.G.; Barnard, P.J. Localization of the Mdx Mutation within the Mouse Dystrophin Gene. *EMBO J.* **1988**, *7*, 3017–3021.
99. Yucel, N.; Chang, A.C.; Day, J.W.; Rosenthal, N.; Blau, H.M. Humanizing the Mdx Mouse Model of DMD: The Long and the Short of It. *NPJ Regen. Med.* **2018**, *3*, 4, doi:10.1038/s41536-018-0045-4.
100. Stedman, H.H.; Sweeney, H.L.; Shrager, J.B.; Maguire, H.C.; Panettieri, R.A.; Petrof, B.; Narusawa, M.; Leferovich, J.M.; Sladky, J.T.; Kelly, A.M. The Mdx Mouse Diaphragm Reproduces the Degenerative Changes of Duchenne Muscular Dystrophy. *Nature* **1991**, *352*, 536–539, doi:10.1038/352536a0.
101. Hammers, D.W.; Hart, C.C.; Matheny, M.K.; Wright, L.A.; Armellini, M.; Barton, E.R.; Sweeney, H.L. The D2.Mdx Mouse as a Preclinical Model of the Skeletal Muscle Pathology Associated with Duchenne Muscular Dystrophy. *Sci. Rep.* **2020**, *10*, 14070, doi:10.1038/s41598-020-70987-y.
102. Coley, W.D.; Bogdanik, L.; Vila, M.C.; Yu, Q.; Van Der Meulen, J.H.; Rayavarapu, S.; Novak, J.S.; Nearing, M.; Quinn, J.L.; Saunders, A.; et al. Effect of Genetic Background on the Dystrophic Phenotype in Mdx Mice. *Hum. Mol. Genet.* **2016**, *25*, 130–145, doi:10.1093/hmg/ddv460.
103. Rodrigues, M.; Echigoya, Y.; Maruyama, R.; Lim, K.R.Q.; Fukada, S.-I.; Yokota, T. Impaired Regenerative Capacity and Lower Revertant Fibre Expansion in Dystrophin-Deficient Mdx Muscles on DBA/2 Background. *Sci. Rep.* **2016**, *6*, 38371, doi:10.1038/srep38371.
104. Fukada, S.; Morikawa, D.; Yamamoto, Y.; Yoshida, T.; Sumie, N.; Yamaguchi, M.; Ito, T.; Miyagoe-Suzuki, Y.; Takeda, S.; Tsujikawa, K.; et al. Genetic Background Affects Properties of Satellite Cells and Mdx Phenotypes. *Am. J. Pathol.* **2010**, *176*, 2414–2424, doi:10.2353/ajpath.2010.090887.
105. van Putten, M.; Putker, K.; Overzier, M.; Adamzek, W.A.; Pasteuning-Vuhman, S.; Plomp, J.J.; Aartsma-Rus, A. Natural Disease History of the D2-Mdx Mouse Model for Duchenne Muscular Dystrophy. *FASEB J.* **2019**, *33*, 8110–8124, doi:10.1096/fj.201802488R.
106. Flanigan, K.M.; Ceco, E.; Lamar, K.-M.; Kaminoh, Y.; Dunn, D.M.; Mendell, J.R.; King, W.M.; Pestronk, A.; Florence, J.M.; Mathews, K.D.; et al. *LTBP4* Genotype Predicts Age of Ambulatory Loss in Duchenne Muscular Dystrophy: *LTBP4* Genotype in DMD. *Ann. Neurol.* **2013**, *73*, 481–488, doi:10.1002/ana.23819.
107. Bello, L.; Kesari, A.; Gordish-Dressman, H.; Cnaan, A.; Morgenroth, L.P.; Punetha, J.; Duong, T.; Henricson, E.K.; Pegoraro, E.; McDonald, C.M.; et al. Genetic Modifiers of Ambulation in the Cooperative International Neuromuscular Research Group Duchenne Natural History Study: Ambulation in CINRG-DNHS. *Ann. Neurol.* **2015**, *77*, 684–696, doi:10.1002/ana.24370.
108. Massague, J.; Cheifetz, S.; Endo, T.; Nadal-Ginard, B. Type Beta Transforming Growth Factor Is an Inhibitor of Myogenic Differentiation. *Proc. Natl. Acad. Sci.* **1986**, *83*, 8206–8210, doi:10.1073/pnas.83.21.8206.
109. Ignotz, R.A.; Massagué, J. Transforming Growth Factor-Beta Stimulates the Expression of Fibronectin and Collagen and Their Incorporation into the Extracellular Matrix. *J. Biol. Chem.* **1986**, *261*, 4337–4345.

110. Olson, E.N.; Sternberg, E.; Hu, J.S.; Spizz, G.; Wilcox, C. Regulation of Myogenic Differentiation by Type Beta Transforming Growth Factor. *J. Cell Biol.* **1986**, *103*, 1799–1805, doi:10.1083/jcb.103.5.1799.
111. Cohn, R.D.; van Erp, C.; Habashi, J.P.; Soleimani, A.A.; Klein, E.C.; Lisi, M.T.; Gamradt, M.; ap Rhys, C.M.; Holm, T.M.; Loeys, B.L.; et al. Angiotensin II Type 1 Receptor Blockade Attenuates TGF-β–Induced Failure of Muscle Regeneration in Multiple Myopathic States. *Nat. Med.* **2007**, *13*, 204–210, doi:10.1038/nm1536.
112. Mázala, D.A.G.; Novak, J.S.; Hogarth, M.W.; Nearing, M.; Adusumalli, P.; Tully, C.B.; Habib, N.F.; Gordish-Dressman, H.; Chen, Y.-W.; Jaiswal, J.K.; et al. TGF-β–Driven Muscle Degeneration and Failed Regeneration Underlie Disease Onset in a DMD Mouse Model. *JCI Insight* **2020**, *5*, e135703, doi:10.1172/jci.insight.135703.
113. Weir, J.B. de V. New Methods for Calculating Metabolic Rate with Special Reference to Protein Metabolism. *J. Physiol.* **1949**, *109*, 1–9, doi:10.1113/jphysiol.1949.sp004363.
114. Improvement of Dystrophic Muscle Fragility by Short-Term Voluntary Exercise through Activation of Calcineurin Pathway in Mdx Mice | Elsevier Enhanced Reader Available online: https://reader.elsevier.com/reader/sd/pii/S000294401830023 3?token=2E0C80A8AD101EB8258138F5C9FFF3804E15C0D4646014BB8B8DE267022FDA7FE05B41B82AEB0AA42636C50180ECEB56&originRegion=us-east-1&originCreation=20210621152908 (accessed on 21 June 2021).
115. Feske, S.; Rao, A.; Hogan, P.G. The Ca2+–calcineurin–NFAT signalling pathway. In *New Comprehensive Biochemistry*; Krebs, J., Michalak, M., Eds.; Calcium; Elsevier, 2007; Vol. 41, pp. 365–401.
116. Bergeron, R.; Ren, J.M.; Cadman, K.S.; Moore, I.K.; Perret, P.; Pypaert, M.; Young, L.H.; Semenkovich, C.F.; Shulman, G.I. Chronic Activation of AMP Kinase Results in NRF-1 Activation and Mitochondrial Biogenesis. *Am. J. Physiol. Endocrinol. Metab.* **2001**, *281*, E1340-1346, doi:10.1152/ajpendo.2001.281.6.E1340.
117. Ljubicic, V.; Miura, P.; Burt, M.; Boudreault, L.; Khogali, S.; Lunde, J.A.; Renaud, J.-M.; Jasmin, B.J. Chronic AMPK Activation Evokes the Slow, Oxidative Myogenic Program and Triggers Beneficial Adaptations in Mdx Mouse Skeletal Muscle. *Hum. Mol. Genet.* **2011**, *20*, 3478–3493, doi:10.1093/hmg/ddr265.
118. Chakkalakal, J.V. Stimulation of Calcineurin Signaling Attenuates the Dystrophic Pathology in Mdx Mice. *Hum. Mol. Genet.* **2003**, *13*, 379–388, doi:10.1093/hmg/ddh037.
119. Selsby, J.T.; Morine, K.J.; Pendrak, K.; Barton, E.R.; Sweeney, H.L. Rescue of Dystrophic Skeletal Muscle by PGC-1α Involves a Fast to Slow Fiber Type Shift in the Mdx Mouse. *PloS One* **2012**, *7*, e30063, doi:10.1371/journal.pone.0030063.
120. Lusk, G. ANIMAL CALORIMETRY: Twenty-Fourth Paper. ANALYSIS OF THE OXIDATION OF MIXTURES OF CARBOHYDRATE AND FAT. *J. Biol. Chem.* **1924**, *59*, 41–42, doi:10.1016/S0021-9258(18)85293-0.
121. Akinci, B.; Sahinoz, M.; Oral, E. Lipodystrophy Syndromes: Presentation and Treatment. In *Endotext*; Feingold, K.R., Anawalt, B., Boyce, A., Chrousos, G., de Herder, W.W., Dhatariya, K., Dungan, K., Grossman, A., Hershman, J.M., Hofland, J., Kalra, S., Kaltsas, G., Koch, C., Kopp, P., Korbonits, M., Kovacs, C.S., Kuohung, W., Laferrère, B., McGee, E.A., McLachlan, R., Morley, J.E., New,

M., Purnell, J., Sahay, R., Singer, F., Stratakis, C.A., Trence, D.L., Wilson, D.P., Eds.; MDText.com, Inc.: South Dartmouth (MA), 2000.
122. Strakova, J.; Kamdar, F.; Kulhanek, D.; Razzoli, M.; Garry, D.J.; Ervasti, J.M.; Bartolomucci, A.; Townsend, D. Integrative Effects of Dystrophin Loss on Metabolic Function of the Mdx Mouse. *Sci. Rep.* **2018**, *8*, 13624, doi:10.1038/s41598-018-31753-3.
123. Singh, S.; Periasamy, M.; Bal, N.C. Strain Specific Differences in Muscle Ca2+ Transport and Mitochondrial Electron Transport Proteins between FVB/N and C57BL/6J Mice. *J. Exp. Biol.* **2020**, jeb.238634, doi:10.1242/jeb.238634.
124. Keeley, T.P.; Siow, R.C.M.; Jacob, R.; Mann, G.E. Reduced SERCA Activity Underlies Dysregulation of Ca^{2+} Homeostasis under Atmospheric O_2 Levels. *FASEB J.* **2018**, *32*, 2531–2538, doi:10.1096/fj.201700685RRR.
125. Qaisar, R.; Bhaskaran, S.; Ranjit, R.; Sataranatarajan, K.; Premkumar, P.; Huseman, K.; Van Remmen, H. Restoration of SERCA ATPase Prevents Oxidative Stress-Related Muscle Atrophy and Weakness. *Redox Biol.* **2019**, *20*, 68–74, doi:10.1016/j.redox.2018.09.018.
126. Gailly, P.; De Backer, F.; Van Schoor, M.; Gillis, J.M. In Situ Measurements of Calpain Activity in Isolated Muscle Fibres from Normal and Dystrophin-Lacking Mdx Mice. *J. Physiol.* **2007**, *582*, 1261–1275, doi:10.1113/jphysiol.2007.132191.
127. Li, F.-Z.; Cai, P.-C.; Song, L.-J.; Zhou, L.-L.; Zhang, Q.; Rao, S.-S.; Xia, Y.; Xiang, F.; Xin, J.-B.; Greer, P.A.; et al. Crosstalk between Calpain Activation and TGF-B1 Augments Collagen-I Synthesis in Pulmonary Fibrosis. *Biochim. Biophys. Acta BBA - Mol. Basis Dis.* **2015**, *1852*, 1796–1804, doi:10.1016/j.bbadis.2015.06.008.
128. Yeh, Y.-H.; Kuo, C.-T.; Chan, T.-H.; Chang, G.-J.; Qi, X.-Y.; Tsai, F.; Nattel, S.; Chen, W.-J. Transforming Growth Factor-β and Oxidative Stress Mediate Tachycardia-Induced Cellular Remodelling in Cultured Atrial-Derived Myocytes. *Cardiovasc. Res.* **2011**, *91*, 62–70, doi:10.1093/cvr/cvr041.
129. Heydemann, A.; Ceco, E.; Lim, J.E.; Hadhazy, M.; Ryder, P.; Moran, J.L.; Beier, D.R.; Palmer, A.A.; McNally, E.M. Latent TGF-β–Binding Protein 4 Modifies Muscular Dystrophy in Mice. *J. Clin. Invest.* **2009**, *119*, 3703–3712, doi:10.1172/JCI39845.
130. Timpani, C.A.; Hayes, A.; Rybalka, E. Revisiting the Dystrophin-ATP Connection: How Half a Century of Research Still Implicates Mitochondrial Dysfunction in Duchenne Muscular Dystrophy Aetiology. *Med. Hypotheses* **2015**, *85*, 1021–1033, doi:10.1016/j.mehy.2015.08.015.
131. Hughes, M.C.; Ramos, S.V.; Turnbull, P.C.; Rebalka, I.A.; Cao, A.; Monaco, C.M.F.; Varah, N.E.; Edgett, B.A.; Huber, J.S.; Tadi, P.; et al. Early Myopathy in Duchenne Muscular Dystrophy Is Associated with Elevated Mitochondrial H2 O2 Emission during Impaired Oxidative Phosphorylation. *J. Cachexia Sarcopenia Muscle* **2019**, *10*, 643–661, doi:10.1002/jcsm.12405.
132. Bukowska, A.; Lendeckel, U.; Bode-Böger, S.M.; Goette, A. Physiologic and Pathophysiologic Role of Calpain: Implications for the Occurrence of Atrial Fibrillation: Physiologic and Pathophysiologic Role of Calpain. *Cardiovasc. Ther.* **2012**, *30*, e115–e127, doi:10.1111/j.1755-5922.2010.00245.x.
133. Galluzzi, L.; Kepp, O.; Chan, F.K.-M.; Kroemer, G. Necroptosis: Mechanisms and Relevance to Disease. *Annu. Rev. Pathol.* **2017**, *12*, 103–130, doi:10.1146/annurev-pathol-052016-100247.
134. Festjens, N.; Vanden Berghe, T.; Vandenabeele, P. Necrosis, a Well-Orchestrated Form of Cell Demise: Signalling Cascades, Important Mediators and Concomitant

Immune Response. *Biochim. Biophys. Acta* **2006**, *1757*, 1371–1387, doi:10.1016/j.bbabio.2006.06.014.
135. Peth, A.; Nathan, J.A.; Goldberg, A.L. The ATP Costs and Time Required to Degrade Ubiquitinated Proteins by the 26 S Proteasome. *J. Biol. Chem.* **2013**, *288*, 29215–29222, doi:10.1074/jbc.M113.482570.
136. Smith, I.J.; Dodd, S.L. Calpain Activation Causes a Proteasome-Dependent Increase in Protein Degradation and Inhibits the Akt Signalling Pathway in Rat Diaphragm Muscle. *Exp. Physiol.* **2007**, *92*, 561–573, doi:10.1113/expphysiol.2006.035790.
137. Pant, M.; Sopariwala, D.H.; Bal, N.C.; Lowe, J.; Delfín, D.A.; Rafael-Fortney, J.; Periasamy, M. Metabolic Dysfunction and Altered Mitochondrial Dynamics in the Utrophin-Dystrophin Deficient Mouse Model of Duchenne Muscular Dystrophy. *PLOS ONE* **2015**, *10*, e0123875, doi:10.1371/journal.pone.0123875.
138. Estler, C.-J. Efficiency of Thermoregulation in Acutely Cold-Exposed Young and Old Mice. *Life Sci.* **1971**, *10*, 1291–1298, doi:10.1016/0024-3205(71)90328-6.
139. McLaren, A. Some Causes of Variation of Body Temperature in Mice. *Q. J. Exp. Physiol. Cogn. Med. Sci.* **1961**, *46*, 38–45, doi:10.1113/expphysiol.1961.sp001513.
140. Nowack, J.; Giroud, S.; Arnold, W.; Ruf, T. Muscle Non-Shivering Thermogenesis and Its Role in the Evolution of Endothermy. *Front. Physiol.* **2017**, *8*, 889, doi:10.3389/fphys.2017.00889.
141. Morse, C.I.; Smith, J.; Denny, A.; Tweedale, J.; Searle, N.D. Gastrocnemius Medialis Muscle Architecture and Physiological Cross Sectional Area in Adult Males with Duchenne Muscular Dystrophy. *J. Musculoskelet. Neuronal Interact.* **2015**, *15*, 154–160.
142. Carroll, K.; Yiu, E.M.; Ryan, M.M.; Kennedy, R.A.; de Valle, K. The Effects of Calf Massage in Boys with Duchenne Muscular Dystrophy: A Prospective Interventional Study. *Disabil. Rehabil.* **2020**, 1–7, doi:10.1080/09638288.2020.1753829.
143. Friedrich, O.; von Wegner, F.; Chamberlain, J.S.; Fink, R.H.A.; Rohrbach, P. L-Type Ca2+ Channel Function Is Linked to Dystrophin Expression in Mammalian Muscle. *PLoS ONE* **2008**, *3*, e1762, doi:10.1371/journal.pone.0001762.
144. Pertille, A.; de Carvalho, C.L.T.; Matsumura, C.Y.; Neto, H.S.; Marques, M.J. Calcium-Binding Proteins in Skeletal Muscles of the Mdx Mice: Potential Role in the Pathogenesis of Duchenne Muscular Dystrophy. *Int. J. Exp. Pathol.* **2010**, *91*, 63–71, doi:10.1111/j.1365-2613.2009.00688.x.
145. Edwards, J.N.; Friedrich, O.; Cully, T.R.; von Wegner, F.; Murphy, R.M.; Launikonis, B.S. Upregulation of Store-Operated Ca2+ Entry in Dystrophic Mdx Mouse Muscle. *Am. J. Physiol. Cell Physiol.* **2010**, *299*, C42-50, doi:10.1152/ajpcell.00524.2009.
146. Bal, N.C.; Gupta, S.C.; Pant, M.; Sopariwala, D.H.; Gonzalez-Escobedo, G.; Turner, J.; Gunn, J.S.; Pierson, C.R.; Harper, S.Q.; Rafael-Fortney, J.A.; et al. Is Upregulation of Sarcolipin Beneficial or Detrimental to Muscle Function? *Front. Physiol.* **2021**, *12*, 633058, doi:10.3389/fphys.2021.633058.
147. Fu, M.; Bombardier, E.; Gamu, D.; Tupling, A.R. Phospholamban and Sarcolipin Prevent Thermal Inactivation of Sarco(Endo)Plasmic Reticulum Ca2+-ATPases. *Biochem. J.* **2020**, *477*, 4281–4294, doi:10.1042/BCJ20200346.
148. Flepisi, T.B.; Lochner, A.; Huisamen, B. The Consequences of Long-Term Glycogen Synthase Kinase-3 Inhibition on Normal and Insulin Resistant Rat

Hearts. *Cardiovasc. Drugs Ther.* **2013**, *27*, 381–392, doi:10.1007/s10557-013-6467-8.
149. Hamstra, S.I.; Kurgan, N.; Baranowski, R.W.; Qiu, L.; Watson, C.J.F.; Messner, H.N.; MacPherson, R.E.K.; MacNeil, A.J.; Roy, B.D.; Fajardo, V.A. Low-Dose Lithium Feeding Increases the SERCA2a-to-Phospholamban Ratio, Improving SERCA Function in Murine Left Ventricles. *Exp. Physiol.* **2020**, *105*, 666–675, doi:10.1113/EP088061.
150. National Center for Biotechnology Information PubChem Compound Summary for CID 11313622, Tideglusib 2021.
151. Horrigan, J.; Gomes, T.B.; Snape, M.; Nikolenko, N.; McMorn, A.; Evans, S.; Yaroshinsky, A.; Della Pasqua, O.; Oosterholt, S.; Lochmüller, H. A Phase 2 Study of AMO-02 (Tideglusib) in Congenital and Childhood-Onset Myotonic Dystrophy Type 1 (DM1). *Pediatr. Neurol.* **2020**, *112*, 84–93, doi:10.1016/j.pediatrneurol.2020.08.001.
152. Pascual-Gilabert, M.; López-Castel, A.; Artero, R. Myotonic Dystrophy Type 1 Drug Development: A Pipeline toward the Market. *Drug Discov. Today* **2021**, S1359-6446(21)00160–4, doi:10.1016/j.drudis.2021.03.024.
153. Wong, S.H.; McClaren, B.J.; Archibald, A.D.; Weeks, A.; Langmaid, T.; Ryan, M.M.; Kornberg, A.; Metcalfe, S.A. A Mixed Methods Study of Age at Diagnosis and Diagnostic Odyssey for Duchenne Muscular Dystrophy. *Eur. J. Hum. Genet.* **2015**, *23*, 1294–1300, doi:10.1038/ejhg.2014.301.
154. Dutta, S.; Sengupta, P. Men and Mice: Relating Their Ages. *Life Sci.* **2016**, *152*, 244–248, doi:10.1016/j.lfs.2015.10.025.